Evaluation of Ba deficient $NdBaCo_2O_{5+\delta}$ oxide as cathode material for IT-SOFC

A. Donazzi[a*], *R. Pelosato*[b*], *G. Cordaro*[b], *D. Stucchi*[b], *C. Cristiani*[b], *G. Dotelli*[b], *I. Natali Sora*[c]

[a] Dipartimento di Energia, Politecnico di Milano, Via Lambruschini 4, 20156 Milano, Italy

[b] Dipartimento di Chimica Materiali e Ingegneria Chimica "Giulio Natta", Politecnico di Milano, Piazza Leonardo da Vinci 32, 20133 Milano, Italy

[c] INSTM R. U. and Università di Bergamo, Dipartimento di Ingegneria e Scienze Applicate, Viale Marconi 5, 24044 Dalmine (BG), Italy

*corresponding authors:

Alessandro Donazzi

Dipartimento di Energia

Via Lambruschini 4, 20156 Milano (Italy)

Phone: 0039 02 2399 8651

Fax: 0039 02 2399 3318

e-mail: alessandro.donazzi@polimi.it

Renato Pelosato

Dipartimento di Chimica Materiali e Ingegneria Chimica “G. Natta”

Piazza Leonardo da Vinci 32, 20123 Milano (Italy)

Phone: 0039 02 2399 3232

Fax: 0039 02 7063 8173

e-mail: renato.pelosato@polimi.it

Abstract

Neodymium- and cobalt-based layered perovskite oxides with increasing Ba deficiency ($NdBa_{1-x}Co_2O_{5+\delta}$, x = 0.0 ÷ 0.2) are prepared via solid state firing. The chemical and electrochemical properties of these materials are characterized via XRD, SEM, TG-DTA, 4-probe conductivity measurement and EIS tests on symmetric cells. The maximum tolerated Ba deficiency is slightly below 10%. The compounds crystallize in an ordered layered structure with orthorhombic *Pmmm* (for x = 0 and 0.5) and tetragonal *P4/mmm* (for x = 0.10) crystal lattice. All the compounds show high total conductivity (between 400 and 600 S/cm at 700°C). A remarkable tenfold decrease of the area specific resistance is observed at decreasing the Ba content from 0 to 10%, with the compound at 10% Ba deficiency reaching the best performance (0.1 $\Omega*cm^2$ at 700°C). Detailed equivalent circuit analysis on EIS tests at varying temperature (550 to 700°C) and O_2 content (100% to 5% v/v) reveals that the limiting steps are the transport of oxygen ions within the cathodic phase and across the electrolyte interface at high frequency, and the formation of an oxygen ion at intermediate frequency. The effect of Ba on the electrochemical mechanism is associated with a promotion of the bulk diffusion steps at high frequency.

Keywords: NBC; cathode; IT-SOFC; EIS; kinetics.

1. Introduction

The quest for electrode materials capable of attaining good electrochemical performances in Intermediate Temperature Solid Oxide Fuel Cells (IT-SOFCs) is a key research topic. Recently, attention has been paid to a family of cobalt-based layered perovskite compounds that can be grouped in the general formula $AA'B_2O_{5+\delta}$, where A is a rare earth, A' an alkaline earth, commonly Ba, while the B site is most often occupied by Co ions. Many related compounds with different substitutions on A' and B sites, or both, have been investigated [1, 2]. The essential characteristic of these compounds is the ordering of the A-site cations in alternating layers, A-O, B-O, A'-O, B-O along the *c*-axis of the perovskite lattice [3-5]. Several efforts have been devoted to study the effects that the substitutions have on the crystal structure, the oxygen content, the thermal expansion, the oxygen surface exchange, the electrical conductivity and the electrochemical activity. Very recently, it was found that the defect chemistry of these compounds can be tailored by introducing small changes in the stoichiometry of either A or A' site: in this latter case, partially substituting the A'-site Ba cations with Sr is generally understood to enhance the electrical conductivity [6-8]. Doping the B-site Co cations with transition metals, especially Fe, Cu, Ni or Mn, is adopted to limit the thermal expansion [6, 9-11]; though, high levels of substitution of the Co cation can dramatically affect the electrochemical activity, even conferring anodic properties for use in symmetric SOFCs [12]. A' site under-stoichiometry was first investigated: Ba deficiency ($x = 0 \div 0.08$) in $PrBa_{1-x}Co_2O_{5+\delta}$ caused a shrinkage of the crystal cell size, slightly affected the thermal expansion coefficient, and affected both the electrical conductivity and the electrochemical activity [13-15]. A similar study was performed on $LaBa_{1-x}Co_2O_{5+\delta}$: this compound tolerated a large Ba under-stoichiometry ($x = 0.0 \div 0.15$) without significant modification of the lattice parameters. A monotonic decrease both in the electrical

conductivity and in the ASR was found by increasing the deficiency up to 10% [16]. The results of these investigations could be rationalized based on the dominant charge compensation mechanism. Introducing different amounts of deficiency generates metal ion vacancies (v''_{Ba}) in the structure; this loss of charge must be compensated, by generation of either new electronic defects ($Co^{\bullet}_{Co}$) or ionic defects ($v^{\bullet\bullet}_{O}$). Given that the two mentioned defects are the charge carriers of the electronic and the ionic conductivity, the mechanism of charge compensation affects both the electronic conductivity and the ionic conductivity of the under-stoichiometric compounds. Therefore, it is in principle possible to achieve a high cathodic performance by optimizing the amount of defects in the structure of the material, thus minimizing the polarization losses without hindering the electronic conductivity. Among the cobalt based layered perovskite oxides, $NdBaCo_2O_{5+\delta}$ appears to be much less investigated than other oxides, even though it possesses remarkable oxygen surface exchange properties [3, 8, 17-20]. In this paper, we focus on the effects that a cation deficiency on A'-site in the range $0.0 \leq x \leq 0.2$ has on the physico-chemical and the electrochemical properties of $NdBa_{1-x}Co_2O_{5+\delta}$. For each compound, the powders were chemically characterized via X-Ray Diffraction, SEM, TG-DTA analyses and cerimetric titration. The electrochemical properties were evaluated by measuring the total electrical conductivity, via 4-probe method on sintered bars, and the polarization behavior, via Electrochemical Impedance Spectroscopy (EIS) on symmetric cell configuration. For the first time, a mechanistic insight on the effect of Ba deficiency in the oxygen reduction activity of these cathode materials is offered, based on the quantitative analysis of the EIS spectra.

2. Materials and Methods

$NdBa_{1-x}Co_2O_{5+\delta}$ samples with x = 0, 0.05, 0.10 and 0.20 (named after the Ba deficiency NBC0, NBC5, NBC10 and NBC20) were prepared via solid state mixing and firing method. $Nd(NO_3)_3 \cdot 6H_2O$, $Ba(NO_3)_2$, $Co(OCOCH_3)_2 \cdot xH_2O$ salts were used as precursors. The Nd and Co precursors were converted into the corresponding oxides (Nd_2O_3 and Co_3O_4) by proper thermal treatment. $Ba(NO_3)_2$ was heated up at 280°C to remove any absorbed water. The precursors were ball-milled in isopropyl alcohol for 24 h, fired at 800°C for 12 h in air, milled again 24 h in isopropyl alcohol and finally fired twice at 1100°C for 12 h in air with intermediate regrinding. The cooling ramps of the high temperature treatments were kept at 1°C/min to allow for the equilibration of the oxygen content with the surrounding atmosphere. The phase composition of the powders was checked by X-Ray Diffraction (XRD) using a Bruker D8 Advance Diffractometer, with graphite monochromated Cu-Kα radiation. The diffraction patterns were collected in the range 10–80 °2θ with a step of 0.02 °2θ and a counting time of 1 s per step for the phase analyses and 12 s per step for the structural analyses. The XRD data were analyzed using routines available in the GSAS package, including the Rietveld method [21]. XRD analyses were carried out also on mechanical mixtures (50/50 wt%) of the NBC samples with GDC ($Ce_{0.9}Gd_{0.1}O_2$, Sigma Aldrich) and LSGM ($La_{0.8}Sr_{0.2}Ga_{0.8}Mg_{0.2}O_3$, Fuel Cell Materials), to evaluate the occurrence of chemical interactions between the electrolyte and the cathode materials, after firing up to 1100°C in the case of GDC and 1000°C in the case of LSGM.

Thermogravimetric Analyses (TG-DTA) were performed on ca. 40 mg of the NBC samples by a simultaneous TG-DTG Seiko 6300 instrument. In a TG-DTA experiment, the powders were heated in air from room temperature to 850°C at 3°C/min, and then cooled again to room temperature with the same rate.

The oxidation state of cobalt and the oxygen content of all the compounds were estimated by cerimetric redox titrations: ca. 50 mg of powdered sample was dissolved in a 1M HCl solution (about 50 ml) containing a known excess of Fe^{2+} ($FeCl_2 \bullet 4H_2O$) and held a few minutes for the following reaction to occur:

$$Co^{n+} + (n-2)Fe^{2+} \rightarrow Co^{2+} + (n-2)Fe^{3+} \qquad [1]$$

After the reaction, the remaining Fe^{2+} was titrated with a solution of $Ce(SO_4)_2$ in 1M H_2SO_4 using ferroin as indicator; the end-point was evaluated visually by the sudden color change from orange to green. The concentration of $Ce(SO_4)_2$ solution (about 0.01M) was standardized against a sodium oxalate ($Na_2C_2O_4$) solution at 80°C, and was itself used to determine the exact concentration of the starting $FeCl_2 \bullet 4H_2O$ solution (about 0.01M). For each determination, three experiments were carried out.

The electrical conductivity and the polarization resistance of the samples were measured as a function of temperature with a potentiostat/galvanostat (AMEL 7050) equipped with a Frequency Response Analyzer (FRA). The electrical conductivity was measured via a four-electrode DC method on sintered bars (25 mm long, 5 mm wide, 3 mm thick, calcined in air at 1100°C for 4 h) between 25 and 850°C. The calcination temperature was purposely kept at 1100°C, in order for the samples to be representative of the cell electrodes and to avoid volatilization and loss of Co. Though, a temperature of 1100°C was not sufficient to achieve complete sinterization of the bars and residual porosity was present. The porosity of the bars was estimated by comparing the density values measured with the buoyancy balance in ethanol and the values of the theoretical density (ρ_{theor}) calculated from the lattice parameters. On average, 35% porosity resulted for all the samples.

EIS tests were performed using a symmetric cell configuration with GDC as the electrolyte. The GDC pellets (1.1 cm diameter) were fabricated via die-pressing

and calcination (1400°C, 12 h, air). The sinterization of each pellet was verified by comparing the density value measured with the buoyancy balance (7.101 g/cm^3) with the theoretical density (7.159 g/cm^3). 99% of the theoretical density was achieved. A slurry of the cathode material (60 wt% solid content) was prepared from the powders by adding α-terpineol, isopropyl alcohol and ethyl cellulose (76:20:4 relative weights) and stirring the resulting mixture for 2 h. The slurry was then applied on each side of the pellet, dried at 110°C for 12 h in air, and calcined at 1100°C to reach adhesion. To collect the current, Ag meshes were applied with silver paint on both sides of each pellet. The EIS tests were performed between 550 and 750°C, at Open Circuit Voltage (OCV) with 10 mV voltage amplitude and in the frequency range 0.1 Hz – 10 kHz. At all the temperatures, the EIS tests were carried out under air flow (50 Ncc/min) and at different O_2 partial pressure (5%, 10% and 100% v/v). Experiments were also carried out by using He instead of N_2 as the O_2 diluent at 21% and 5% O_2 to verify the impact of mass transfer limitations. The Equivalent Circuit Model (ECM) method was applied with Zview to evaluate the contributions of the physical, chemical and electrochemical steps of the Oxygen Reduction Reaction (ORR) mechanism.

The morphological features of the calcined powders and of the electrodes of the symmetric cells were assessed via Scanning Electron Microscopy (SEM) using a Carl Zeiss EVO50VP instrument equipped with an Energy Dispersive Spectrometer (EDS) for elemental analysis.

3. Results and Discussion

3.1 XRD characterization of the NBC powders

The XRD patterns of the samples obtained after calcination at 1100°C are shown in Figure 1. The pure $NdBa_{1-x}Co_2O_{5+\delta}$ phase is obtained at x = 0 and 0.05 (NBC0 and NBC5), while a trace of an impurity phase is detected in the x = 0.10 sample (NBC10). The same phase is found in larger amount in the x = 0.20 sample (NBC20). This impurity can be identified as $NdCoO_3$ (PDF #00-025-1064). The formation of a secondary phase containing Nd and Co in the 10% deficient compound suggests that the maximum Ba deficiency accepted by $NdBa_{1-x}Co_2O_{5+\delta}$ is slightly lower than 10%: once this threshold is overcome, the Ba-free phase emerges. For this reason, the structural properties were studied only for NBC0, NBC5 and NBC10 materials, and the NBC20 was excluded. All the compounds crystallize in an A-site ordered perovskite structure. The pattern of sample NBC0 can be indexed using a tetragonal unit cell having lattice parameters $a = b = a_p$, $c = 2a_p$ (a_p being the lattice parameter of the cubic perovskite). However, Rietveld refinements using the tetragonal unit cell (*P4/mmm* space group) give somehow unsatisfactory goodness-of-fit parameters, i.e. $\chi^2 = 1.516$, $R_{wp} = 20.56\%$, $R_p = 13.44\%$ and $R_B = 7.24\%$. Closer examination of the diffraction profile evidence the broadening of some reflections, especially that at ca. 1.98 Å, which suggests to index the pattern using an orthorhombic unit cell. Moreover, the presence of a very weak reflection at ca. 7.8 Å indicates doubling of the *b* lattice parameter due to ordering of oxygen vacancies. Rietveld refinements performed using the orthorhombic doubled unit cell a_p x $2a_p$ x $2a_p$ (*Pmmm* space group) and the crystal parameters of $NdBaCo_2O_{5.69}$ [22] give better results, namely $\chi^2 = 1.323$, $R_{wp} = 19.19\%$, $R_p = 11.91\%$ and $R_B = 5.53\%$ (Table 1). The Rietveld refinements were performed using the total oxygen occupancy obtained by the cerimetric titration (see Section 3.2). The structural parameters of NBC5 are similar to those of orthorhombic NBC0, although with a smaller orthorhombic distortion. The pattern of NBC10 show neither a clear peak broadening at 1.98 Å, nor

superstructure reflection. Refinements are performed using a model on the basis of a tetragonal a_p x a_p x $2a_p$ unit cell (*P4/mmm* space group). The final refined cell parameters are reported in Table 1. As shown in Figure 2, the Ba deficiency causes a shrinkage of the structure, mainly due to the *b* parameter, and to a smaller extent to the *a* parameter. The *c* parameter is much less affected. For the NBC10 sample, the refined occupancy of Ba gave value 0.922(3), corresponding to a threshold of ca. 8%. This result is in agreement with the value found by Pang et al. [15] in similar $PrBa_{1-x}Co_2O_{5+\delta}$ compounds. The similarity between the ion sizes of Nd and Pr seems to validate a value around 8% for the tolerated Ba deficiency in $NdBa_{1-x}Co_2O_{5+\delta}$. Despite the similarity of the ion sizes, however, the transition observed in NBC from the orthorhombic structure to the tetragonal one is not reported for the $PrBa_{1-x}Co_2O_{5+\delta}$ cathodes, whose structure maintains unaltered at varying the amount of Ba (orthorhombic in [15] and tetragonal in [13]). The transition is associated to a significant change in the concentration of oxygen vacancies: a lower amount of oxygen vacancies gives rise to an orthorhombic structure, while a higher amount results in a tetragonal structure. Therefore, the results of the XRD analysis suggest that the concentration of oxygen vacancies progressively increases passing from NBC0 to NBC10.

The powders of the four compounds were also analyzed with a scanning electron microscope to access the morphology. Good homogeneity is found for all the samples both in composition and size (Fig. 3a, the NBC10 sample is taken as a representative example): although the aggregates are slightly irregular in shape, the grains have similar size, in the range of few micrometers. Overall, after calcination at 1100°C, the powders show a continuous structure with diffuse open porosity. Additionally, the EDS spectra are also reasonably in line with the expected compositions, namely 51.2% Co, 25.3% Nd and 23.5% Ba on molar basis for NBC10,

estimated by neglecting the O signal and the signals of Au and Al, these latter being respectively due to the plating and to the holder. Only in the case of the NBC20 sample (Fig. 3b), particles of a Co-rich phase with traces of Nd and Ba (98.5% Co, 1% Nd and 0.5% Ba on molar basis) can be detected, which are not observed in the XRD and which confirm that a too high Ba deficiency promotes the separation of secondary phases.

The pieces of evidence collected by the XRD and the SEM analyses allowed to discard the NBC20 sample as a valid cathode. Hence, the compatibility between the cathodes and the electrolyte materials was evaluated exclusively on the NBC0, NBC5 and NBC10 samples. The occurrence of chemical interactions with either GDC or LSGM was assessed by preparing 50/50 wt% mixtures of the NBC powders and the electrolyte powders. The mixtures were fired at increasing temperatures and the recovered powders were analyzed via XRD. All the NBC/LSGM mixtures fired at 1000°C for 5 h (Fig. 4) reveal the formation of new phases: new peaks are detected in the XRD patterns, which can be assigned to $BaNdGa_3O_7$ (PDF #00-024-0110) and/or $BaLaGa_3O_7$ (PDF #00-024-0107). Traces of the same reaction products are found also at lower temperature, 900°C for 12 h, confirming the fast chemical reaction between LSGM and the NBC compounds. A previous report [3] showed no reactivity between $NdBaCo_2O_{5+\delta}$ and LSGM: though, the thermal treatments adopted in the reference were much shorter than the present ones (1100°C for 0.5 h and 1000°C for 3 h), likely suggesting that longer times would have eventually revealed some reactivity. In the present case, temperatures lower than 900°C were not investigated as they were not suitable for obtaining good adhesion of the cathode material onto the electrolyte. These observations suggest to avoid the use of NBC compounds with LSGM electrolyte without the use of a proper barrier layer.

The XRD patterns of the NBC/GDC mixtures, treated under the same conditions as the LSGM (12 h at 900°C and 5 h at 1000°C), show neither the appearance of new peaks, nor any visible alteration in the position of the peaks. Moreover, the mixtures fired at 1000°C were further heated at 1100°C for 5 hours: also in this case, no visible changes are present in the XRD patterns (Fig. 5). These results clearly show that a very good chemical compatibility exists between the prepared NBC compounds and the GDC electrolyte. The GDC electrolyte was therefore chosen for the electrochemical characterization, in order to avoid the formation of secondary phases during the measurements. Overall, the XRD spectra of both the LSGM- and the GDC-based mechanical mixtures also indicate that the Ba deficiency does not affect the interactions with the two electrolytes in a measurable extent.

3.2 Measurement of conductivity and oxygen-exchanging properties

The results of the cerimetric titration are summarized in Table 2. The titration allows to directly measure the amounts of Co^{3+} and Co^{4+} ions present in each $NdBa_{1-x}Co_2O_{5+\delta}$ sample, and therefore the average oxidation state of the Co is determined. The oxygen content is calculated from the stoichiometry, given the oxidation states of Nd and Ba (Nd^{3+} and Ba^{2+}). The content of oxygen vacancies is estimated as the difference of the oxygen content from the stoichiometric value of 6. Upon decreasing the Ba content, the average oxidation state of cobalt and the number of oxygen vacancies both increase, while the oxygen content decreases. A high number of vacancies is beneficial for the electrochemical activity of the material, which is related to the capability of introducing, transporting and desorbing oxygen inside and outside the structure; as well, the fraction of Co^{4+} ions must be sufficiently high, being

the inclusion and transportation mechanism associated to the redox couple Co^{4+}/Co^{3+}. The increase in the Ba deficiency increases both these parameters, leading to a favorable and synergistic effect. It is thus interesting to explore the relationship of the Ba content with the capability of the material to exchange oxygen.

This capability was first investigated via thermogravimetric analysis in air, up to 850°C. For each sample, the measured weight change (Fig. 6a) is directly related to the change in the oxygen content and to the oxidation state of cobalt (Fig. 6b). At increasing temperature, all the NBC formulations experience first a moderate loss of oxygen between 50 and 250°C, which is followed by a steady, linear decrease up to 850°C. A peak of oxygen gain, and weight gain, was always detected around 275°C: an analogous observation was reported in the TG analyses of NBC samples by Kim and Irvine [17]. After reaching of stable weight conditions, further cycling revealed fully reproducible characteristics for all the three samples. Upon decreasing the oxygen content, the oxidation state of cobalt decreases, as a consequence of the reduction of the Co^{4+} ions to Co^{3+}. Only at temperatures higher than 800-850°C, well beyond the limit for IT-SOFCs, further reduction of the Co^{3+} to Co^{2+} ions causes the oxidation state to fall below the average state of 3, indicating the complete depletion of Co^{4+} ions and the activation of the Co^{3+}/Co^{2+} redox couple. In the intermediate temperature branch (300 – 500°C), the NBC10 sample experiences the sharpest loss of oxygen, followed by that of NBC5 and that of NBC0. In the high temperature branch (500 – 800°C), the NBC10 sample maintains the highest loss rate, followed by that of NBC0, while that of NBC5 moderates. In the whole temperature range, the NBC10 sample loses 0.25 oxygen atoms per unit formula, 0.18 the NBC5 sample and 0.16 the NBC0 and 0.18. Consistently, up to 700°C, the NBC10 sample loses the highest weight fraction, followed by NBC5 and NBC0. These results clearly indicate

that the increase in the Ba deficiency progressively increases also the capability of desorbing oxygen from the lattice.

The desorption of lattice oxygen affects the structural and the electrical properties of the material. The electrical behavior of the samples was then investigated in terms of total electrical conductivity as a function of temperature, under air flow conditions. The results of the total electrical conductivity measurements between 50 and 850°C are reported in Figure 7. The values reported are referred to the dense structure of the bar by normalizing the measured values of conductivity σ_m by the solid fraction of the bar ($1 - \varepsilon_{void}$), according to the formula [23]:

$$\sigma = \frac{\sigma_m}{1 - \varepsilon_{void}} \qquad [2]$$

On average, the conductivity values of all the samples largely meet the requirements for application in IT-SOFCs (over 100 S/cm at 600-700°C), in line with literature results obtained with similar double-layered perovskite oxides [3, 15, 16, 24, 25] and with the measurements reported for NBC samples [8, 26, 27]. In the low temperature region, at T < 250°C, a moderate loss of conductivity is observed for NBC0 and NBC10, while the conductivity maintains almost constant in NBC5. At temperatures higher than 250°C, all the samples experience a decrease of conductivity with increasing temperature, showing a metal-type behavior. A comparison with the results of Figure 6b reveals a strong similarity of the conductivity curves with those of the oxygen loss, with respect both to temperature thresholds and detail features (e.g. the local maxima at around 275°C). This analogy is well explained by considering the following oxygen desorption stoichiometry, expressed in Kröger-Vink notation:

$$2Co_{Co}^{\bullet} + O_O^x \leftrightarrow \frac{1}{2}O_2 + 2Co_{Co}^x + v_O^{\bullet\bullet} \qquad [3]$$

In the equation, the reduction of Co ions (i.e. Co^{4+}, positive charge carriers, $Co_{Co}^{\bullet}$) at the expenses of lattice oxygen ions (O_O^x) generates molecular oxygen, positive oxygen vacancies ($v_O^{\bullet\bullet}$) and Co ions with no surplus charge (Co^{3+}). Upon increasing the temperature, the sample loses oxygen, decreasing its oxidation state: this, in turn, generates vacancies and decreases the number of p-type electronic charge carriers, which are responsible for the electrical conductivity of the sample.

Along with the general evolution of the conductivity curves, it is important to focus on the differences observed at varying the Ba deficiency. The NBC5 sample shows the highest conductivity in the whole temperature range, followed by NBC0 and NBC10 (insert). The effect of Ba on the NBC conductivity can be rationalized by considering that the cationic deficiency on Ba sites generates negative v''_{Ba} defects in the structure; these defects can be compensated either by generation of an equal number of oxygen vacancies $v_O^{\bullet\bullet}$, or by oxidation of two B-site cobalt ions ($Co_{Co}^{\bullet}$). The first mechanism hinders the electrical conductivity, although it enhances the oxygen transport capability. In contrast, the second mechanism benefits the electrical conductivity by increasing the number of electronic charge carriers, but hinders the oxygen transport function. The experimental measurements suggest that the latter mechanism is active passing from x = 0.05 to x = 0.10, and that the high Ba deficiency of the NBC10 sample could be accompanied by a more favorable oxygen exchange activity, as first suggested by the results of the thermogravimetric analyses (Fig. 6a). Additionally, to better elucidate the electrical behavior of the NBC samples, a comparison with literature of $PrBa_{1-x}Co_2O_{5+\delta}$ cathodes is addressed. A variety of trends are reported for the conductivity of PBC cathodes. A maximum (at x = 0.05) in

the conductivity at decreasing Ba content (x = 0 – 0.10) was reported by Dong et al. [13]; in analogous experiments, Pang et al. [15] found a minimum in the electrical conductivity at varying the Ba deficiency (x = 0 – 0.08), located at x = 0.03; finally, Jiang et al. [14] found an increase of the conductivity up to 0.10 Ba deficiency. Differently from Nd, Pr is reported to exhibit both the 3+ oxidation state and the 4+ oxidation state, as shown via XPS in Refs. [9, 14, 28] for double perovskites (up to 20% Pr^{4+} and 80% Pr^{3+}) and in Refs. [29, 30] for disordered perovskites; in the case of Nd, the 4+ oxidation state has never been reported in perovskite oxides and exclusively the 3+ is present. This is a key difference: in Pr-based compounds, both Co and Pr can be oxidized to compensate the Ba vacancies, hence the electronic charge carriers can be generated by Co and Pr, in different extent. Depending upon the preparation history and calcination conditions (e.g. maximum temperature and heating/cooling rate), Pr^{4+} and Co^{4+} are present in different amounts, therefore resulting in a different influence on the compensation mechanism. In the case of Nd, the occurrence of a single oxidation specie guarantees that the compensation mechanism only involves the Co^{3+}/Co^{4+} couple and the oxygen vacancies. In order to clarify if the compensation mechanism of NBC cathodes acts primarily via the oxygen vacancy formation or via the Co oxidation, it is convenient to analyze the electrochemical ORR activity via EIS investigation.

3.3 EIS characterization of the NBC samples

The individuation of the optimal cathodic performance is the result of a balance. A high conductivity must be accompanied by a favorable activity as oxygen reducing catalyst: these two characteristics can benefit from the lack of lattice Ba, although excess deficiency may become detrimental. To elucidate the general effect

of Ba on NBC, the ORR activity was first evaluated via EIS tests on symmetric NBC/GDC/NBC cells, in the temperature range between 750 and 550°C, at OCV and under air flow. Experiments were also carried out by using He instead of N_2 as the O_2 diluent to verify the impact of internal mass transfer limitation and individuate the corresponding effect on the impedance arcs. For each cell, the microstructure was analyzed with SEM after the measurement. A section of the cell based on the NBC10 cathode is reported in Figure 3c, and almost identical pictures were taken for the other samples. For each of the cells, a detail of the cathode electrolyte/interface is provided in the panels d to f, wherein the thickness of electrodes and the particle size are better appreciated. The pictures confirm that no significant difference is found in the microstructure at increasing the Ba deficiency: a fair contact is realized between the NBC particles and the GDC electrolyte. Although the continuity can be improved by using a finer grain size, a good porosity is achieved, which guarantees a low impact of gas diffusive limitations. The images also show that all the electrodes have an average thickness of ~30 μm. The porosity was determined from the electrode weight and thickness via the density values (Table 1), and amounted to ~45%. Overall, these results confirm that the symmetric cells have almost equal morphological features (layer thickness, porosity, grain size and connectivity) and therefore allow for a fair comparison of the EIS results.

The ASR values estimated from the EIS tests performed with air are summarized in Figure 8a. The best performance is achieved by the NBC10 sample for both the polarization resistance (0.1 $\Omega*cm^2$ at 700°C) and the apparent activation energy (1.18 eV), followed by the NBC5 sample (1.28 eV and 0.25 $\Omega*cm^2$ at 700°C). The stoichiometric NBC0 sample has the lowest activity and the larger activation energy (1.31 eV and 0.99 $\Omega*cm^2$ at 700°C). The NBC10 sample is suitable for the application as a cathode in IT-SOFCs, being the polarization resistance lower than the

target 0.15 Ω*cm^2 at 700°C, suggested by the guidelines of Ref. [31]. A comparison with the most relevant literature results obtained on NBC cathodes (Fig. 8b) confirms that the activation energies of the three samples are well within the range extracted from the published data, which spans between 0.9 eV and 1.42 eV with most of the values being close to 1.18 eV. With respect to the activity, although a direct comparison can be only regarded as qualitative due to the differences in microstructure and preparation method, the ASR of the NBC10 sample is in good agreement with that of the work by Kim and Irvine [17], while the ASRs of NBC5 and NBC0 reach higher levels. This result could be a consequence of the firing temperature chosen to achieve the adhesion of the electrodes in the symmetric cell, which is higher (1100°C) than the common value (1000°C) adopted in the works and which could have led to a lower extension of the active area.

With reference to the effect of the Ba content, the ASR decreases tenfold passing from the NBC0 sample to the NBC10, suggesting that the optimal conditions are met at the highest Ba deficiency. This result is widely in line with the results found on similar perovskites based on rare earths [14-16, 24, 32]: for these materials, it is generally understood that a certain amount of Ba deficiency is beneficial, thanks to the introduction of oxygen vacancies in the lattice. On Pr and La perovskites, a steady decrease of the polarization resistance is typically identified as a function of the Ba deficiency (~0.1 for Pr [15] and 0.1 – 0.15 for La [16]): nonetheless, a reduction of 10 times of the polarization resistance at decreasing the Ba content is likely a unique characteristic of Nd-based cathodes and constitutes a most significant result, which distinguishes the use of Nd from other rare earths. On analogous Pr-based cathodes the polarization resistance almost halves passing from 0 to 0.1 Ba deficiency in [14], whereas the variation reported in Refs. [13] and [15] is lower, ~1.2 and ~1.6 times respectively. The smaller effect reported for Pr compared to Nd can be

rationalized based on the presence of the additional route for the compensation of the Ba vacancies given by double valence of Pr cations, aside of the route associated to the Co cations: the first possibility is absent in the case of Nd and a more marked effect of the Ba understoichiometry is observed. Additionally, a progressive decrease of the apparent activation energy is expected upon decreasing the Ba content. In the present case, the decrease of the apparent activation energies is well within the range reported for double-perovskites: Pang et al. [15] found a progressive decrease from 1.19 eV to 1.05 eV in $PrBa_{1-x}Co_2O_{5+\delta}$ samples upon varying the Ba content from 0 to 0.15; a variation between 1.17 eV and 1.20 eV was found by the same authors when passing from 0 to 0.15 Ba deficiency in $LaBa_{1-x}Co_2O_{5+\delta}$ cathodes. The observation of the lowest polarization resistance at the highest Ba deficiency is consistent with the results of the TGA analyses (Fig. 6), which show a higher capability of NBC10 in exchanging molecular O_2, as well as with the results of the XRD analyses (Fig. 1) and of the cerimetric titrations (Tab. 2), which indicate the occurrence of a transition from the orthorhombic to the tetragonal structure accompanied by an increase of the oxygen vacancies. A picture emerges wherein the tenfold reduction of the polarization resistance is connected to and enhanced by the structural transition. On the one hand, the results suggest that the maximum activity for $NdBa_{1-x}Co_2O_{5+\delta}$ cathodes is almost achieved at around 10%; on the other hand, they indicate that the compensation mechanism active in the 5 – 10% deficiency range is the one wherein the vacancies are preferably formed.

Overall, when comparing the NBC samples of Figure 8a, it is very important to note that the ASR values are representative of the intrinsic chemical reactivity of the materials, given that mass transport limitations were experimentally proven to be negligible in the presence of air: indeed, as shown in Figure 12b for the NBC10 sample, almost no difference is found when switching from N_2 to He. The same

behavior was verified in the case of all the other samples. This latter observation confirms that Ba influences some steps in the ORR mechanism. In order to gain a deeper insight into the chemical effect of Ba, the NBC10 and the NBC5 sample were further investigated in detail by performing the EIS measurements at varying O_2 content between 100% and 5% between 700°C and 550°C.

3.4 EIS investigation on the NBC10 sample

The results of the EIS experiments carried out in air and under varying O_2 content are reported in Figures 9 and 10 for the NBC10 sample. At all the temperatures, the impedance spectra were analyzed by application of the Equivalent Circuit Method (ECM) based on a circuit of the type $LR_{Ohm}(R_{HF}Q_{HF})(R_{MF}Q_{MF})(R_{LF}Q_{LF})$. L is the inductance caused by the electrical equipment and by the lead wires, R_{Ohm} is the ohmic resistance mainly due to the electrolyte, while the three remaining RQ elements are associated with processes occurring in the electrodes at different characteristic frequencies. This circuit is commonly adopted in the analysis of the properties of perovskite oxides: the high frequency arc (HF) is associated to transfer processes that involve the inclusion of oxygen ions either at the interface with the electrolyte or in the bulk of the cathode structure; the middle frequency arc (MF) is related to electrode processes, such as the dissociative adsorption of oxygen, the formation of adsorbed oxygen ions, or the surface diffusion of oxygen adatoms; the low frequency arc (LF) is due to mass diffusive transport processes, either internal (intra-porous) or external (across the interphase boundary layer). It is very important to note that, in the case of the NBC10 sample, the circuit adopted is the one with the lowest number of elements and fitting parameters which guarantees a solid and physically sound interpretation of the

spectra. A very satisfactory fitting is obtained at all temperatures and all O_2 partial pressures with the 3 arcs model. The results are represented as lines in the figures. For the experiments in air, Table 3 summarizes the values of the circuit elements fitted by the model, as well as the values of the corresponding capacitances and relaxation frequencies. Table 4 reports the values of the same parameters for the experiment at varying of the O_2 content performed at 650°C, which is fully representative of all the analogous experiments at other temperatures. For each process, the resistance values obtained from the best fits are plotted in Arrhenius form as a function of the inverse temperature, in order to evaluate the activation energy (Figure 11d). The reaction orders n of O_2 are estimated according to the inverse relationship between the resistance and the reaction rate (Eq. 4). They are reported for each temperature in Fig. 11a-c.

$$R_i \propto P_{O_2}^{-n} \qquad [4]$$

The experimental EIS spectra show that one single depressed arc is always observed. At decreasing the temperature and the O_2 concentration, the polarization resistance increases. The inspection of the phase curves as a function of the frequency (Fig. 12a) reveals that the growth of the impedance arcs involves primarily the low frequency zone, which extends up to 0.1 Hz when moving to 550°C and 5% O_2, and keeps almost unaltered in the high frequency region at 5 kHz. The phase analysis also shows that the main variation is localized in the middle frequency region, where a peak rises and shifts backward upon decreasing the temperature (and the P O_2). Only at 700°C and 5% O_2 content, a second, smaller arc appears in the 1 – 0.1 Hz frequency range. In this case, as reported in Figure 12b, the second arc can be unambiguously associated to the internal diffusive mass transport, given that its amplitude changes upon substituting N_2 with He. This behavior is common in the case

of MIEC cathodes, wherein the whole electrode volume is involved in the reaction process and a separated diffusive arch is seldom distinguished, except at the lowest O_2 partial pressure [33, 34]. Nonetheless, the impact of the internal diffusion phenomena is limited, as verified by the resistance values of Tables 3 and 4 (between 0.012 – 0.039 $\Omega*cm^2$ passing from 0.21 to 0.05 O_2 v/v at 650°C) and as expected from the porosity (45%) and the thickness of the electrode (30 μm). Consistently with the association of the LF arc to slow diffusive effects, high values of capacitance (3 – 7 F/cm^2) and characteristic frequency (4 – 5 Hz) are calculated. The association is also confirmed by the almost null activation energy (0.1 eV, Fig. 11d) and by the order of reaction observed at varying O_2 content, which is comprised between 0.83 and 0.94, very close to the first order expected from diffusive effects.

From a mechanistic viewpoint, a precise association of the HF and MF arcs with a reaction step requires the reaction orders to be determined together with the activation energies. For the HF process, the values of the capacitance and of the relaxation frequency obtained in the fitting (10^{-3} – 10^{-4} F/cm^2 at 1 – 5 kHz) suggest the association with an ionic transport step. This association is confirmed by the activation energy of 1 eV estimated at all the concentration of O_2 (Fig. 11d) and, above all, by the very small reaction order found for O_2 at all the temperature levels (Fig. 11a), which is comprised between 0.02 and 0.12. This latter is a strong indication that the HF arc is associated with the process of ion transport from the bulk of the cathode phase to the interface with the electrolyte phase, followed by charge transfer across the interface. The following reaction steps are generally used to describe the process [35]:

$$O_O^x \text{ (NBC bulk)} \leftrightarrow O_O^x \text{ (NBC/GDC interface)} \qquad [5]$$

$$O_O^x \text{ (NBC/GDC interface)} \leftrightarrow O_O^x \text{ (GDC bulk)} \qquad [6]$$

Other authors find very similar pieces of evidence when exploring the kinetics of double-layer perovskites doped with rare earth. For instance, Amin and Karan [36] observed a zero order dependence of the HF arc the with $LaBaCo_2O_{5+\delta}$ cathodes, while Shi et al. found a 0.18 dependence on $EuBaCo_2O_{5+\delta}$ cathodes at 700°C [37]. Similarly, Pang et al. [15] discussed a zero order process on symmetrical cells with $PrBa_{1-x}Co_2O_{5+\delta}$ cathodes under almost identical conditions compared to the present ones, estimating values of capacitance between 10^{-3} – 10^{-5} F/cm^2 at 10 to 1 kHz between 650 and 700°C.

In the case of the MF arc, an activation energy of 1.30 – 1.35 eV is estimated between 100 and 5% O_2 partial pressure (Fig. 11d). The reaction order falls within 0.26 and 0.27 between 700 and 600°C (Fig. 11b). The values of capacitance and relaxation frequencies (10^{-2} – 10^{-3} F/cm^2, at 10^2 – 10 Hz, Tables 3 and 4) are consistent with a charge transfer process occurring at the electrode. These pieces of evidence suggest that the MF process can be identified as a charge transfer process wherein an oxygen ion is generated in the cathode phase via reaction between an oxygen adatom and a vacancy, according to the following stoichiometry:

$$O^* + 2e^- + v_O^{\bullet\bullet} \leftrightarrow O_O^x \qquad [7]$$

This process is in line with the overall picture that emerges from Eq. 5 to 7, wherein the adsorbed O species, formed via fast O_2 dissociative adsorption, is first turned into an electroactive oxygen ion, included in the NBC10 phase (Eq. 7), successively transported through the lattice bulk up to the GDC interface (Eq. 5), and finally transferred across the interface (Eq. 6). Upon further decreasing the temperature to 550°C, the rate-limiting step of the MF arc changes, as indicated by the change in the associated reaction order, which passes to a value of 0.47. This values is representative of a dissociative adsorption step that occurs on the cathode surface:

$$O_2 + * \leftrightarrow 2O^* \qquad [8]$$

This step was recently found to limit the ORR mechanism of stoichiometric $LaBaCo_2O_{5+\delta}$ cathodes between 750 and 600°C [38]. A very similar shift from an order of 0.25 to an order of 0.47 was reported by Chen et al. [39] on $PrBaCo_2O_{5+\delta}$ cathodes when passing from 500 to 450°C. Additionally, several other authors working on double-layered perovskites report a variation in one or more kinetic steps upon changing either the P_{O2} or the temperature [37, 40]. It is worthy to note that a change in the determining step should be accompanied by a variation in the activation energy: in the present case, such a change is scarcely seen, due to the absence of additional experiments at temperatures close to or lower than 550°C. Nonetheless, the results indicate that the dissociative adsorption step (8) should have a higher activation energy than the ion inclusion one, so that it becomes limiting upon decreasing the temperature.

3.5 EIS investigation of the NBC5 sample

The kinetic effect of Ba understoichiometry on the electrocatalytic activity of the NBC cathodes is better appreciated by examining the results of the EIS experiments, carried out under air flow at varying the O_2 partial pressure from 100% to 5% between 700°C and 550°C. The results are summarized in Figure 13: for the sake of clarity, the results of the tests at variable P O_2 are reported only at 650°C, a case that is fully representative of all the other temperatures. The numerical results calculated with Zview are summarized in Table 5 and 6, with respect to the fitting of the circuit elements, and in Figure 14a-c, in terms of orders of reaction and activation energy. The first, fundamental difference between the EIS results of the NBC10 and the NBC5 sample is the choice of the equivalent circuit: in the case of NBC5, only a

circuit with four RQ elements consistently fits the arcs and allows for a good match between the model and the data under all the explored conditions. Indeed, exclusively with this kind of circuit, the physico-chemical consistency of some parameters can be respected, above all the relaxation frequency, which decreases with a decrease of the O_2 partial pressure (Table 6) and of the temperature (or keeps almost constant, as in the case of the non-activated diffusive arc, Table 5), as a consequence of the drop of the intrinsic rate.

Also in the case of the NBC5 sample, the EIS spectra present only one depressed arc. The low frequency region is again associated to the internal diffusive mass transport: consistently, the process is almost non activated, a first order dependence on O_2 is found and high capacitive and high frequency values are estimated (10 – 2 F/cm^2 at 1 Hz). However, differently from the NBC10 sample, the experimental data and the phase plot (Fig. 14d) show that, upon decreasing the temperature, the EIS arcs grow in the high frequency region, while the low frequency region maintains almost constant at around 1 Hz. As clearly seen in Figure 14d, going from 700 to 550°C a phase peak develops in the high frequency region in addition to the one that grows in the middle frequency region, which is also observed in NBC10. This is the most relevant difference between the NBC10 sample and the NBC5: an additional arc is present at high frequency, whose resistance progressively increases upon decreasing the temperature. The analysis of the reaction order and the activation energy reveals that a first high frequency arc is present (HF_1) whose activation energy is 1.2 eV and whose dependency on O_2 maintains closely between 0.10 and 0.12 (Fig. 14a, full symbols). The capacity values are in the range $2 \cdot 10^{-4}$ – $8 \cdot 10^{-5}$ F/cm^2 and the frequency between 5 and 1 kHz (Tables 5 and 6). The reaction order suggests that the HF_1 process can be associated to a charge transfer process occurring at the interface and involving oxygen ion, as the one already described in Equation (6) of oxygen

transfer across the TPB interface with inclusion in the electrolyte bulk. For the second high frequency arc (HF_2), an activation energy of ~1.1 eV is estimated, with a reaction order closer to zero (0.06 – 0.08). The capacity values are in the range 10^{-4} – 10^{-5} F/cm^2 and the frequency is around 10 kHz. The zero order dependency suggests that the step described in Equation (5) can be associated to this arc: an association with the crossing of grain boundaries, as observed on $PrBaCo_2O_{5+\delta}$ cathodes [39] is unlikely, given that much smaller capacities and lower temperatures are expected. The MF frequency arc has the same association already observed for the NBC10 sample: an activation energy of 1.1 – 1.2 eV, with a dependence on O_2 of 0.25 and capacities of 10^{-2} – 10^{-3} F/cm^2 at 100 – 10 Hz.

Overall, the results of the EIS analysis suggest that the decrease in the Ba content promotes the steps at high frequency, by decreasing the polarization resistance associated to the transfer of oxygen ions, either inside the cathode phase or across the interface. At 5% Ba deficiency these two steps appear to be slower and more distinguishable, whereas at 10% Ba deficiency the difference is almost absent: that is, in this latter case, the step of diffusion of oxygen ions within the lattice of the NBC phase becomes less resistive. This result is in full agreement with the picture provided by the structural transition from the orthorhombic structure of the sample at 5% Ba deficiency, which has a lower amount of oxygen vacancies and slower kinetics, to the tetragonal structure of the sample at 10% Ba deficiency, which has a higher amount of vacancies and therefore a faster rate of oxygen diffusion. The result also agrees well with the increase of the oxygen vacancies suggested by the TG and by the conductivity measurements in the range 5 to 10% Ba deficiency. From a theoretical viewpoint, the comparison between the results of the numerical analyses performed on the samples at 5% and 10% Ba deficiency allows to identify the mechanistic effect of Ba in the oxygen reduction mechanism, a key-role being played by the choice of

the equivalent circuits which require the lowest number of parameters to fit the arcs while maintaining a physically sound basis.

4. Conclusions

The effect of the A-site Ba-deficiency on the crystal structure and the electrochemical properties of $NdBa_{1-x}Co_2O_{5+\delta}$ double-layered perovskite oxides (x = 0 ÷ 0.20) was investigated. The Ba deficiency affects the cell dimensions by reduction of the *b* lattice parameter, and by increase of the mean oxidation state of Co and increase of the oxygen vacancies. Although the highest total electrical conductivity is met at a Ba deficiency equal to 5% (750 S/cm at 700°C), ASR investigation reveals that a 10 times reduction of the polarization resistance is achieved passing from 0 to 10% Ba understoichiometry, a value at which the optimal electrocatalytic activity in the oxygen reduction process is realized (0.1 $\Omega*cm^2$ at 700°C). Coupling the total conductivity tests with thermogravimetric and EIS tests suggests that the metal vacancies introduced by Ba are mainly compensated via the introduction of novel oxygen vacancies, and, to a minor extent, by the formation of charge carriers by oxidation of Co ions. A detailed EIS analysis via the equivalent circuit method reveals that the effect of Ba is mainly related to processes occurring at high frequency, which tend to become less resistive upon decreasing the Ba content. Specifically, at high frequency the polarization is mainly contributed by oxygen ion diffusion and transfer across the interface, whereas at middle frequency the formation of an oxygen ion and its inclusion in the cathode phase are limiting. The decrease in the Ba content promotes the steps at high frequency, possibly related to the bulk diffusion of oxygen towards the interface with GDC.

References

[1] D.J.L. Brett, A. Atkinson, N.P. Brandon, S.J. Skinner, Chemical Society Reviews, 37 (2008) 1568.

[2] E.V. Tsipis, V.V. Kharton, Journal of Solid State Electrochemistry, 12 (2008) 1367-1391.

[3] J.H. Kim, A. Manthiram, J. Electrochem. Soc., 155 (2008) B385.

[4] A. Tarancón, M. Burriel, J. Santiso, S.J. Skinner, J.A. Kilner, Journal of Materials Chemistry, 20 (2010) 3799.

[5] A. Tarancón, S.J. Skinner, R.J. Chater, F. Hernández-Ramírez, J.A. Kilner, Journal of Materials Chemistry, 17 (2007) 3175.

[6] S. Choi, S. Yoo, J. Kim, S. Park, A. Jun, S. Sengodan, J. Kim, J. Shin, H.Y. Jeong, Y. Choi, G. Kim, M. Liu, Scientific Reports, 3 (2013).

[7] J.H. Kim, M. Cassidy, J.T.S. Irvine, J. Bae, Chemistry of Materials, 22 (2010) 883-892.

[8] S. Yoo, S. Choi, J. Kim, J. Shin, G. Kim, Electrochimica Acta, 100 (2013) 44-50.

[9] F. Jin, H. Xu, W. Long, Y. Shen, T. He, Journal of Power Sources, 243 (2013) 10-18.

[10] J. Kim, S. Choi, S. Park, C. Kim, J. Shin, G. Kim, Electrochimica Acta, 112 (2013) 712-718.

[11] F. Wang, D. Chen, Z. Shao, Electrochimica Acta, 103 (2013) 23-31.

[12] S. Sengodan, S. Choi, A. Jun, T.H. Shin, Y.-W. Ju, H.Y. Jeong, J. Shin, J.T.S. Irvine, G. Kim, Nature Materials, 14 (2015) 205-209.

[13] F. Dong, M. Ni, Y. Chen, D. Chen, M.O. Tade, Z. Shao, Journal of Materials Chemistry A, 2 (2014) 20520-20529.

[14] L. Jiang, F. Li, T. Wei, R. Zeng, Y. Huang, Electrochimica Acta, 133 (2014) 364-372.

[15] S. Pang, X. Jiang, X. Li, Q. Wang, Z. Su, Journal of Power Sources, 204 (2012) 53-59.

[16] S.L. Pang, X.N. Jiang, X.N. Li, H.X. Xu, L. Jiang, Q.L. Xu, Y.C. Shi, Q.Y. Zhang, Journal of Power Sources, 240 (2013) 54-59.

[17] J.H. Kim, J.T.S. Irvine, International Journal of Hydrogen Energy, 37 (2012) 5920-5929.

[18] A.C. Tomkiewicz, M. Meloni, S. McIntosh, Solid State Ion., 260 (2014) 55-59.

[19] W. Wang, T. Peh, S. Chan, T. Zhang, Solid Oxide Fuel Cells 11 (Sofc-Xi), 25 (2009) 2277-2281.

[20] K. Zhang, L. Ge, R. Ran, Z. Shao, S. Liu, Acta Materialia, 56 (2008) 4876-4889.

[21] A.C. Larson, R.B.V. Dreele, in, 2004.

[22] J.C. Burley, J.F. Mitchell, S. Short, D. Miller, Y. Tang, J. Solid State Chem., 170 (2003) 339-350.

[23] J. Wright, A.V. Virkar, Journal of Power Sources, 196 (2011) 6118-6124.

[24] X. Jiang, Y. Shi, W. Zhou, X. Li, Z. Su, S. Pang, L. Jiang, Journal of Power Sources, 272 (2014) 371-377.

[25] J. Wang, F. Meng, T. Xia, Z. Shi, J. Lian, C. Xu, H. Zhao, J.-M. Bassat, J.-C. Grenier, International Journal of Hydrogen Energy, 39 (2014) 18392-18404.

[26] T. Broux, M. Bahout, J.M. Hanlon, O. Hernandez, S. Paofai, A. Berenov, S.J. Skinner, Journal of Materials Chemistry A, 2 (2014) 17015-17023.

[27] J.H. Kim, L. Mogni, F. Prado, A. Caneiro, J.A. Alonso, A. Manthiram, J. Electrochem. Soc., 156 (2009) B1376.

[28] F. Jin, Y. Shen, R. Wang, T. He, Journal of Power Sources, 234 (2013) 244-251.

[29] Y. Hinatsu, M. Itoh, N. Edelstein, J. Solid State Chem., 132 (1997) 337-341.

[30] S. Majumdar, M.R. Lees, G. Balakrishnan, D.M. Paul, Journal of Physics-Condensed Matter, 15 (2003) 7585-7590.

[31] B.C.H. Steele, Solid State Ion., 86-8 (1996) 1223-1234.

[32] C. Setevich, L. Mogni, A. Caneiro, F. Prado, J. Electrochem. Soc., 159 (2012) B73.

[33] S.B. Adler, Chem. Rev., 104 (2004) 4791-4843.

[34] M. Koyama, C.J. Wen, T. Masuyama, J. Otomo, H. Fukunaga, K. Yamada, K. Eguchi, H. Takahashi, J. Electrochem. Soc., 148 (2001) A795-A801.

[35] Y.H. Li, R. Gemmen, X.B. Liu, Journal of Power Sources, 195 (2010) 3345-3358.

[36] R. Amin, B. Kenney, K. Karan, J. Electrochem. Soc., 158 (2011) B1076-B1082.

[37] Z. Shi, T. Xia, F. Meng, J. Wang, J. Lian, H. Zhao, J.M. Bassat, J.C. Grenier, J. Meng, Fuel Cells, 14 (2014) 979-990.

[38] R. Pelosato, A. Donazzi, G. Dotelli, C. Cristiani, I. Natali Sora, M. Mariani, Journal of the European Ceramic Society, 34 (2014) 4257-4272.

[39] D. Chen, R. Ran, K. Zhang, J. Wang, Z. Shao, Journal of Power Sources, 188 (2009) 96-105.

[40] R. Amin, K. Karan, J. Electrochem. Soc., 157 (2010) B285.

Tables

Table 1. Refined structural parameters of the $NdBa_{1-x}Co_2O_{5+\delta}$ samples.

	x = 0	**x = 0.05**	**x = 0.10**
Space group	*Pmmm*	*Pmmm*	*P4/mmm*
a (Å)	3.89921(9)	3.8987(1)	3.89858(4)
b (Å)	7.8107(2)	7.8043(2)	-
c (Å)	7.6125(1)	7.6110(1)	7.6113(1)
V(Å^3)	231.840(8)	231.576(8)	115.683(3)
occupancy Ba	-	-	0.922(3)
ρ_{theor} (g/cm^3)	7.056	6.963	6.865
χ^2	1.323	1.382	1.458
R_{wp} (%)	19.19	20.35	20.80
R_p (%)	11.91	13.04	12.94
R_B (%)	5.53	7.05	7.73

Table 2. Mean oxidation state of cobalt Co^{n+}, Co^{3+} and Co^{4+} ion fraction, oxygen content (5+δ) and oxygen vacancy $v_O^{\bullet\bullet}$ in $NdBa_{1-x}Co_2O_{5+\delta}$.

Sample	**Co^{n+}**	**Co^{3+}**	**Co^{4+}**	**5 + δ**	$v_O^{\bullet\bullet}$
NBC0	3.14	1.72	0.28	5.64	0.36
NBC5	3.17	1.66	0.34	5.62	0.38
NBC10	3.20	1.60	0.40	5.60	0.40

Table 3. Fitting parameters for the EIS tests on the symmetric NBC10/SDC/NBC10 cell with air flow at varying temperature. Operating conditions as in Figure 9.

Element	750°C	700°C	650°C	600°C	550°C
R_{Ohm} (Ω*cm^2)	1.455	2.048	3.006	4.653	7.755
R_{HF} (Ω*cm^2)	0.026	0.047	0.098	0.196	0.400
QPE_{HF}-Q (F*cm^{-2})	3.86E-02	2.54E-02	1.96E-02	8.30E-03	5.47E-03
QPE_{HF}-n	0.687	0.681	0.659	0.681	0.659
C_{HF} (F*cm^{-2})	1.68E-03	1.08E-03	7.71E-04	4.10E-04	2.30E-04
f_{HF} (Hz)	3.61E+03	3.13E+03	2.11E+03	1.98E+03	1.73E+03
R_{MF} (Ω*cm^2)	0.029	0.055	0.112	0.358	0.976
QPE_{MF}-Q (F*cm^{-2})	4.87E-02	4.57E-02	5.50E-02	5.05E-02	3.92E-02
QPE_{MF}-n	0.881	0.834	0.765	0.764	0.752
C_{MF} (F*cm^{-2})	2.00E-02	1.39E-02	1.16E-02	1.47E-02	1.34E-02
f_{MF} (Hz)	2.74E+02	2.09E+02	1.23E+02	3.03E+01	1.22E+01
R_{LF} (Ω*cm^2)	0.010	0.010	0.010	0.012	0.012
QPE_{LF}-Q (F*cm^{-2})	7.08	3.07	5.75	9.55	3.51
QPE_{LF}-n	0.783	0.902	0.906	0.870	0.886
C_{LF} (F*cm^{-2})	3.35	2.10	4.30	6.91	2.34
f_{LF} (Hz)	4.96	7.60	3.53	1.93	5.61

Table 4. Fitting parameters for the EIS tests on the symmetric NBC10/GDC/NBC10 cell at varying O_2 partial pressure at 650°C. Operating conditions as in Figure 10.

Element	100%	21%	10%	5%
R_{HF} (Ω*cm^2)	0.116	0.098	0.097	0.085
QPE_{HF}-Q (F*cm^{-2})	1.90E-02	1.96E-02	1.45E-02	1.17E-02
QPE_{HF}-n	0.643	0.659	0.671	0.778
C_{HF} (F*cm^{-2})	6.38E-04	7.71E-04	5.83E-04	1.62E-03
f_{HF} (Hz)	2.15E+03	2.11E+03	2.81E+03	1.16E+03
R_{MF} (Ω*cm^2)	0.086	0.112	0.143	0.183
QPE_{MF}-Q (F*cm^{-2})	1.01E-01	5.50E-02	5.22E-02	5.31E-02
QPE_{MF}-n	0.670	0.765	0.800	0.810
C_{MF} (F*cm^{-2})	9.68E-03	1.16E-02	1.54E-02	1.81E-02
f_{MF} (Hz)	1.91E+02	1.23E+02	7.19E+01	4.80E+01
R_{LF} (Ω*cm^2)	-	0.010	0.021	0.039
QPE_{LF}-Q (F*cm^{-2})	-	5.75	3.11	4.18
QPE_{LF}-n	-	0.906	0.970	0.840
C_{LF} (F*cm^{-2})	-	4.30	2.840	2.945
f_{LF} (Hz)	-	3.53	2.64	1.37

Table 5. Fitting parameters for the EIS tests on the symmetric NBC5/SDC/NBC5 cell with air flow at varying temperature. Operating conditions as in Figure 13.

Element	750°C	700°C	650°C	600°C	550°C
R_{Ohm} (Ω*cm^2)	1.628	2.286	3.341	5.127	8.415
R_{HF1} (Ω*cm^2)	0.034	0.059	0.190	0.492	1.270
QPE_{HF1}-Q (F*cm^{-2})	2.17E-03	2.55E-03	1.31E-03	7.39E-04	4.92E-04
QPE_{HF1}-n	0.934	0.883	0.835	0.808	0.766
C_{HF1} (F*cm^{-2})	1.11E-03	8.00E-04	2.55E-04	1.12E-04	5.14E-05
f_{HF1} (Hz)	4.22E+03	3.37E+03	3.29E+03	2.89E+03	2.44E+03
R_{HF2} (Ω*cm^2)	-	0.045	0.130	0.293	0.662
QPE_{HF2}-Q (F*cm^{-2})	-	6.92E-04	2.13E-04	1.06E-04	6.05E-05
QPE_{HF2}-n	-	0.943	0.956	0.968	0.948
C_{HF2} (F*cm^{-2})	-	3.69E-04	1.31E-04	7.46E-05	3.05E-05
f_{HF2} (Hz)	-	9.65E+03	9.38E+03	7.28E+03	7.87E+03
R_{MF} (Ω*cm^2)	0.103	0.181	0.409	0.837	2.143
QPE_{MF}-Q (F*cm^{-2})	7.64E-03	6.43E-03	6.12E-03	6.15E-03	6.13E-03
QPE_{MF}-n	0.826	0.796	0.764	0.765	0.787
C_{MF} (F*cm^{-2})	1.69E-03	1.14E-03	9.62E-04	1.22E-03	1.89E-03
f_{MF} (Hz)	9.12E+02	7.73E+02	4.04E+02	1.57E+02	3.93E+01
R_{LF} (Ω*cm^2)	0.005	0.005	0.005	0.005	0.005
QPE_{LF}-Q (F*cm^{-2})	3.009	2.883	2.675	2.738	2.719
QPE_{LF}-n	0.960	0.977	0.969	0.961	0.959
C_{LF} (F*cm^{-2})	2.537	2.599	2.323	2.295	2.259
f_{LF} (Hz)	11.619	13.325	14.458	14.447	14.053

Table 6. Fitting parameters for the EIS tests on the symmetric NBC5/GDC/NBC5 cell at varying O_2 partial pressure at 650°C. Operating conditions as in Figure 13.

Element	100%	21%	10%	5%
R_{HF1} (Ω*cm^2)	0.158	0.190	0.214	0.220
QPE_{HF1}-Q (F*cm^{-2})	1.74E-03	1.31E-03	1.32E-03	1.45E-03
QPE_{HF1}-n	0.793	0.835	0.833	0.859
C_{HF1} (F*cm^{-2})	2.04E-04	2.55E-04	2.56E-04	3.86E-04
f_{HF1} (Hz)	4.95E+03	3.29E+03	2.90E+03	1.87E+03
R_{HF2} (Ω*cm^2)	0.111	0.130	0.129	0.147
QPE_{HF2}-Q (F*cm^{-2})	3.07E-04	2.13E-04	2.46E-04	2.40E-04
QPE_{HF2}-n	0.936	0.956	0.952	0.947
C_{HF2} (F*cm^{-2})	1.51E-04	1.31E-04	1.45E-04	1.35E-04
f_{HF2} (Hz)	9.46E+03	9.38E+03	8.47E+03	8.02E+03
R_{MF} (Ω*cm^2)	0.277	0.409	0.500	0.624
QPE_{MF}-Q (F*cm^{-2})	6.12E-03	6.12E-03	6.73E-03	7.25E-03
QPE_{MF}-n	0.785	0.764	0.744	0.728
C_{MF} (F*cm^{-2})	1.07E-03	9.62E-04	9.46E-04	9.64E-04
f_{MF} (Hz)	5.39E+02	4.04E+02	3.37E+02	2.64E+02
R_{LF} (Ω*cm^2)	-	0.005	0.011	0.019
QPE_{LF}-Q (F*cm^{-2})	-	2.675	4.270	3.967
QPE_{LF}-n	-	0.969	0.755	0.792
C_{LF} (F*cm^{-2})	-	2.323	1.586	2.014
f_{LF} (Hz)	-	14.458	9.076	4.119

Figures

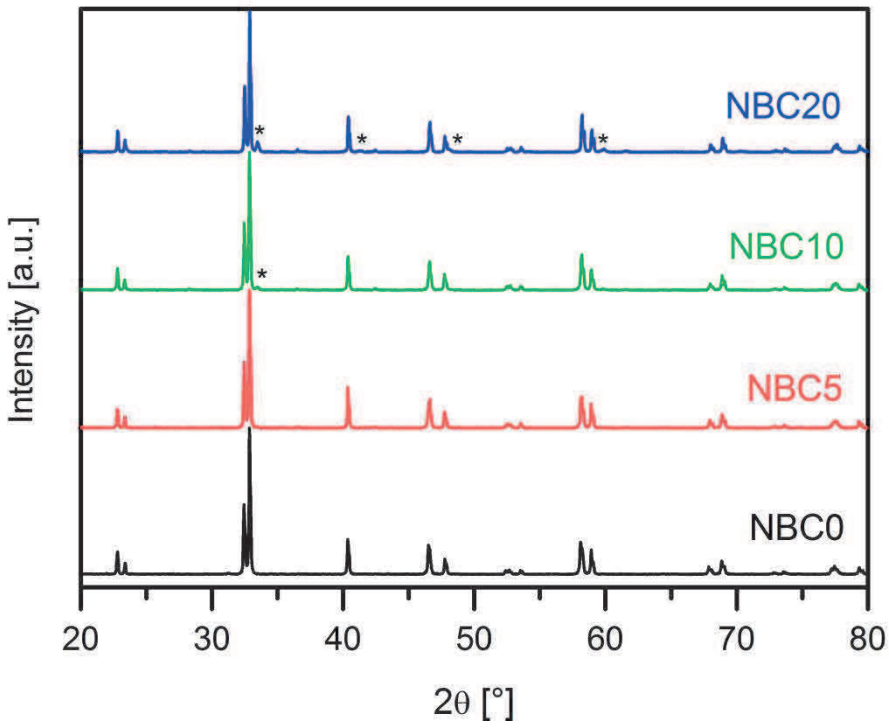

Figure 1

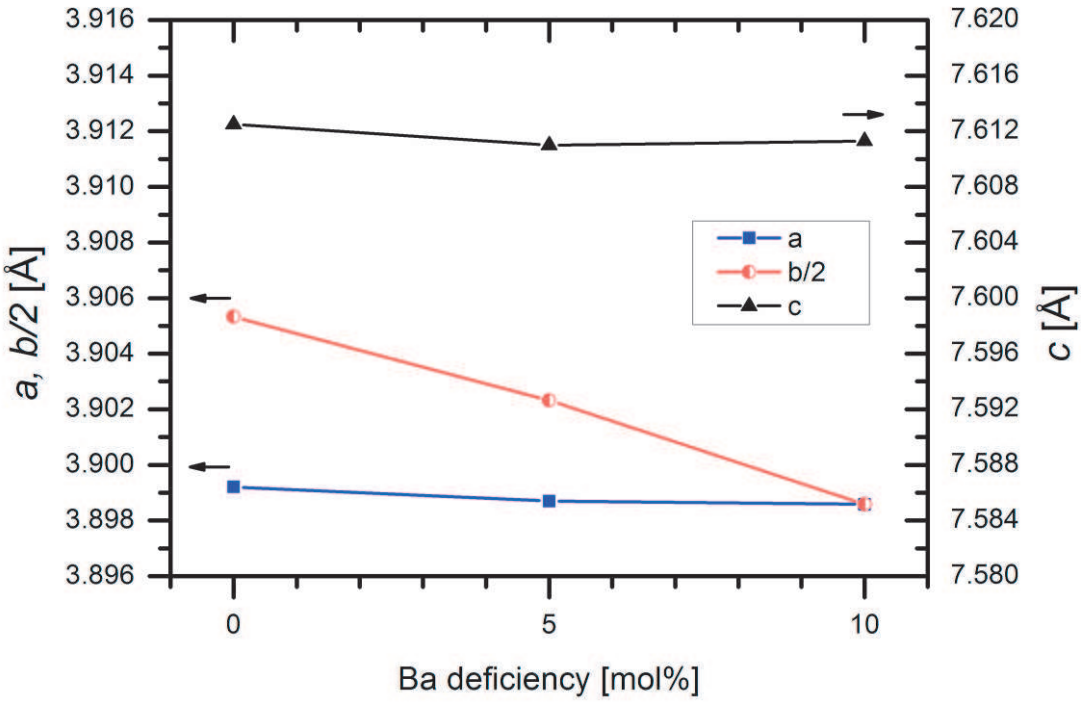
3.916
3.914
3.912
3.910
3.908
3.906
3.904
3.902
3.900
3.898
3.896
a, b/2 [Å]
7.620
7.616
7.612
7.608
7.604
7.600
7.596
7.592
7.588
7.584
7.580
c [Å]
a
b/2
c
0
5
10
Ba deficiency [mol%]

Figure 2

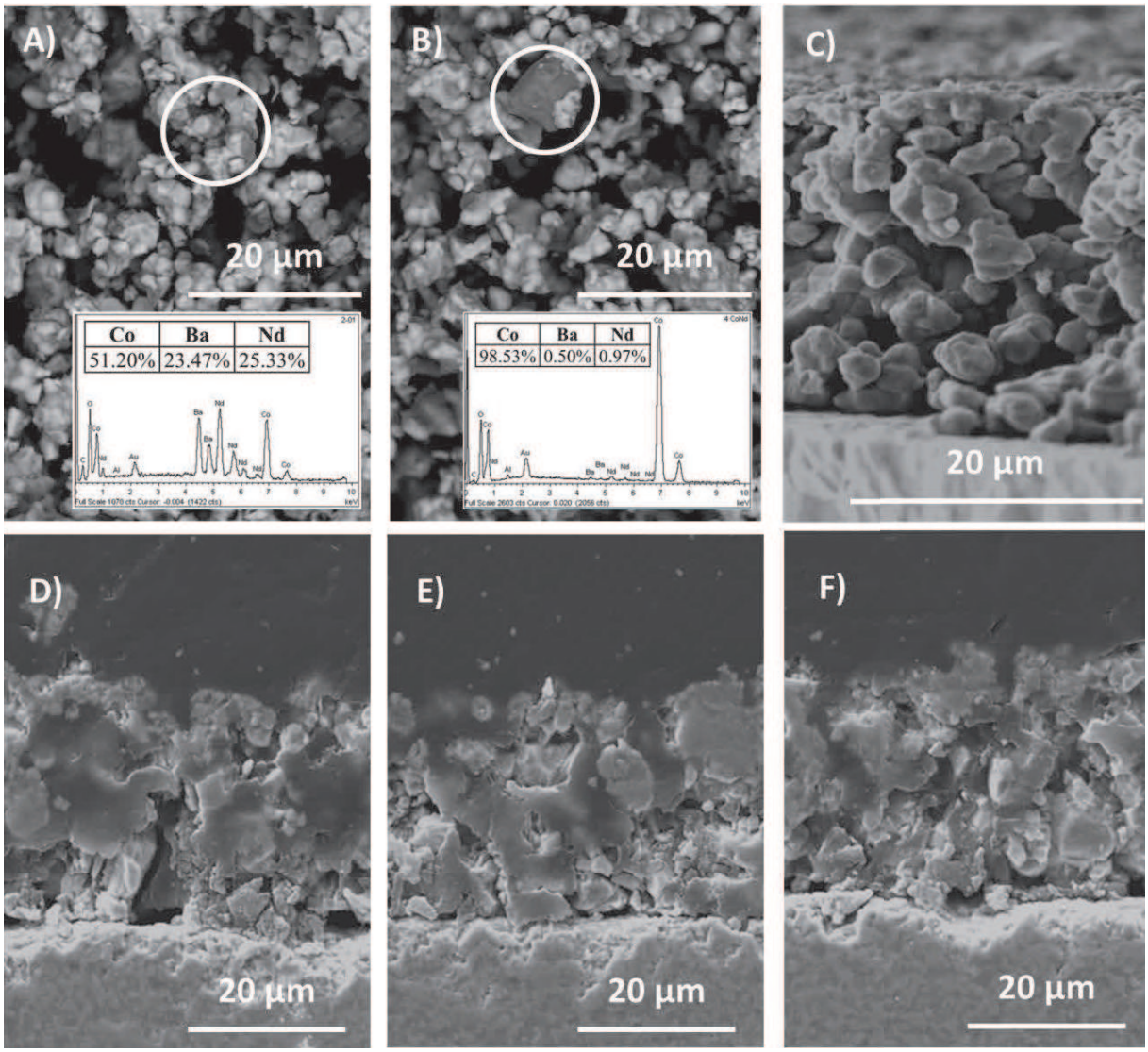
A)
20 µm
Co
Ba
Nd
51.20%
23.47%
25.33%
B)
20 µm
Co
Ba
Nd
98.53%
0.50%
0.97%
C)
20 µm
D)
20 µm
E)
20 µm
F)
20 µm

Figure 3

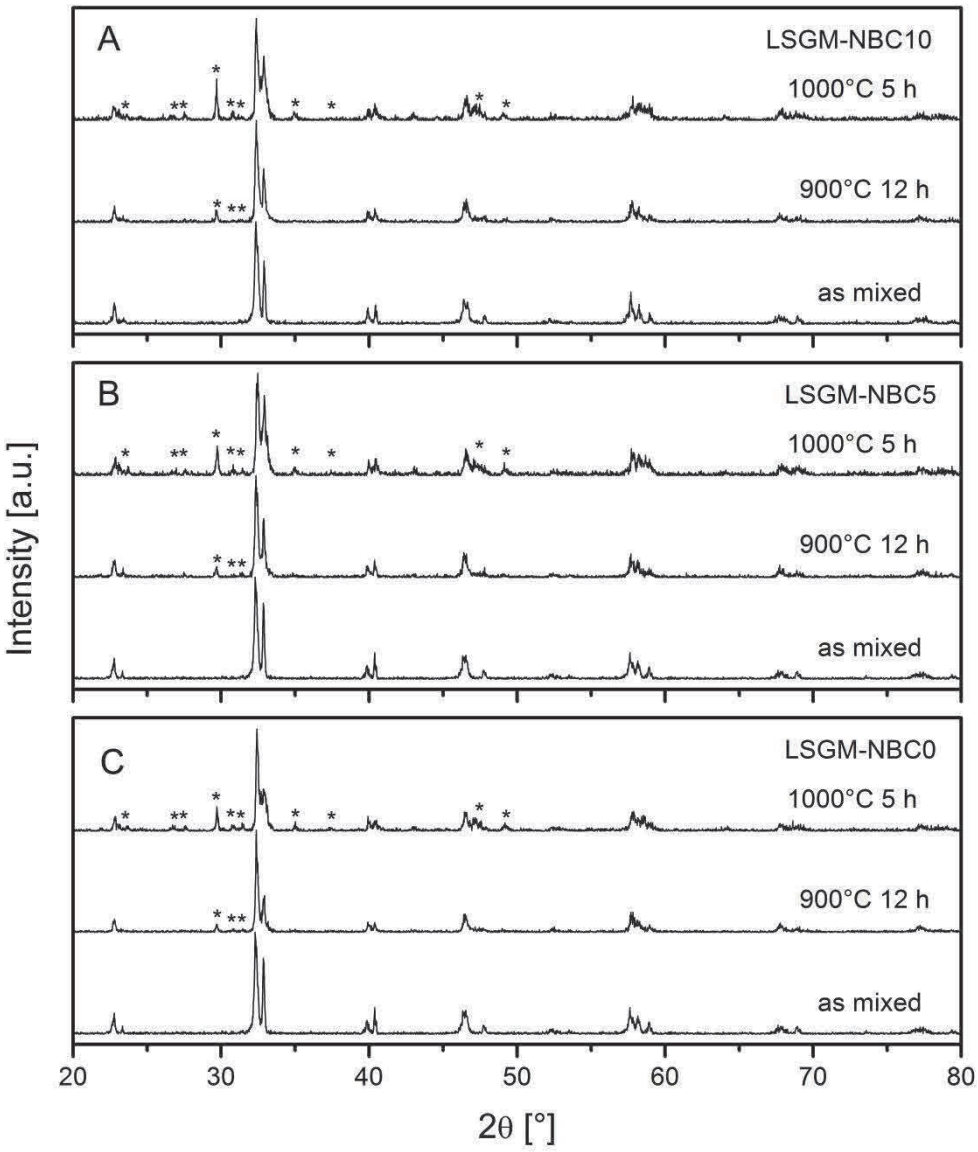
A
LSGM-NBC10
1000°C 5 h
900°C 12 h
as mixed
B
LSGM-NBC5
1000°C 5 h
900°C 12 h
as mixed
C
LSGM-NBC0
1000°C 5 h
900°C 12 h
as mixed
Intensity [a.u.]
20
30
40
50
60
70
80
2θ [°]

Figure 4

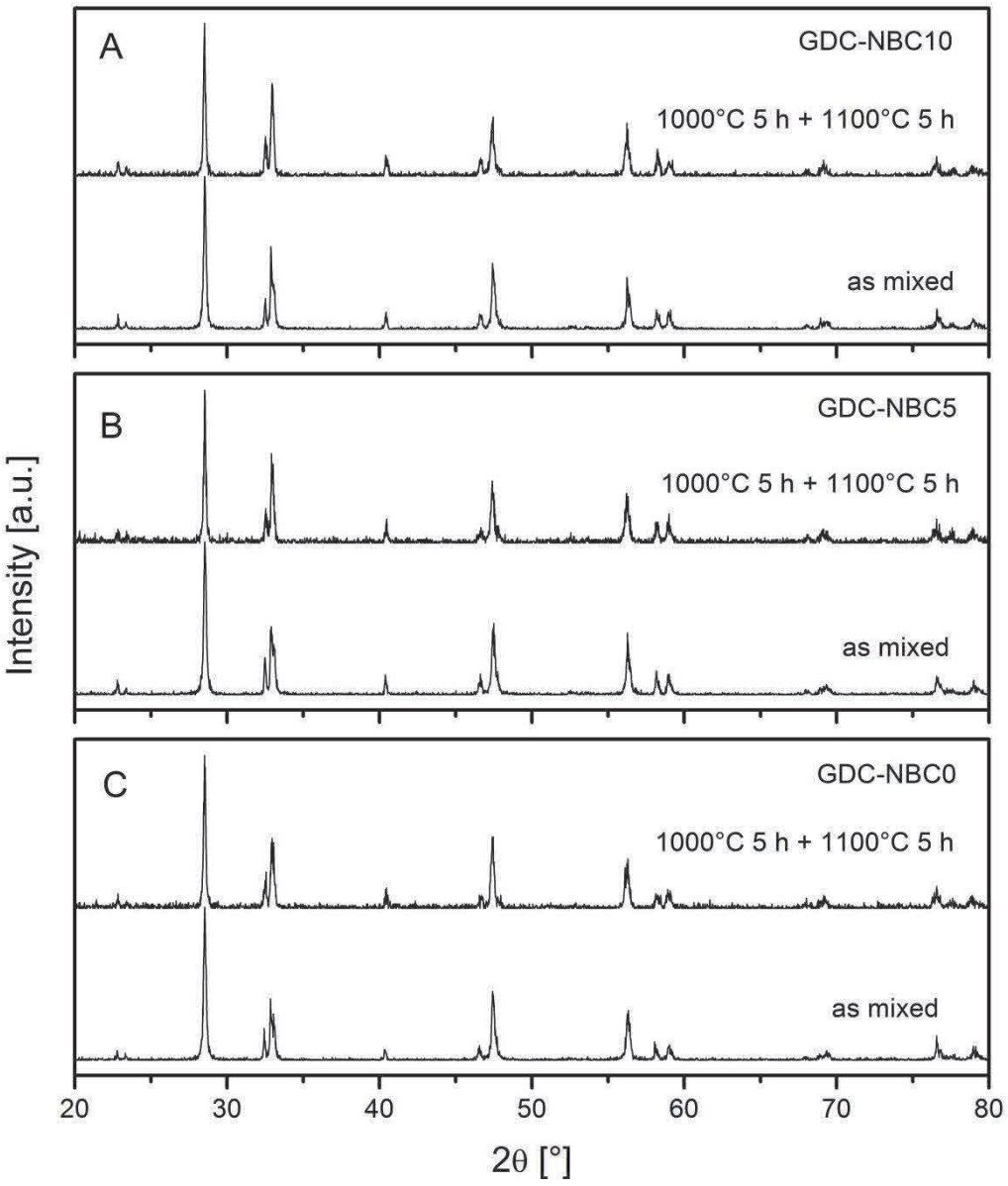
A
GDC-NBC10
1000°C 5 h + 1100°C 5 h
as mixed
B
GDC-NBC5
1000°C 5 h + 1100°C 5 h
as mixed
C
GDC-NBC0
1000°C 5 h + 1100°C 5 h
as mixed
Intensity [a.u.]
20
30
40
50
60
70
80
2θ [°]

Figure 5

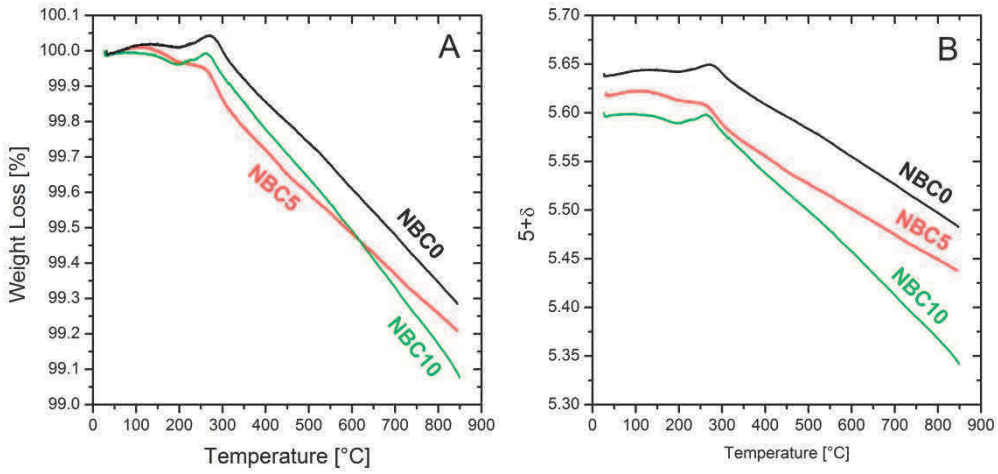

Figure 6

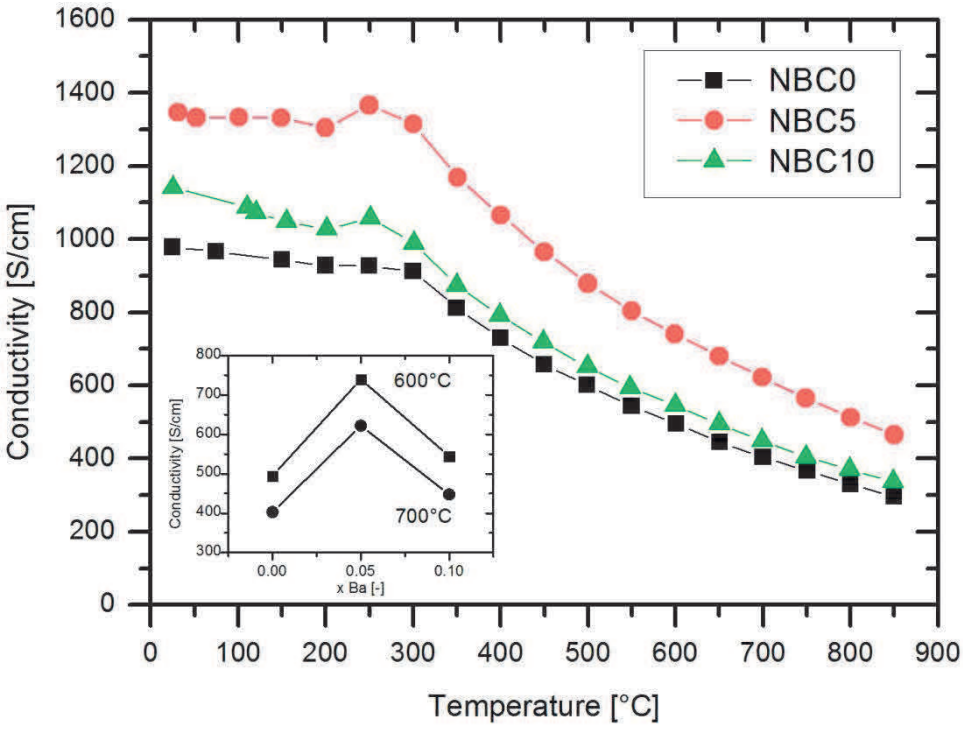

Figure 7

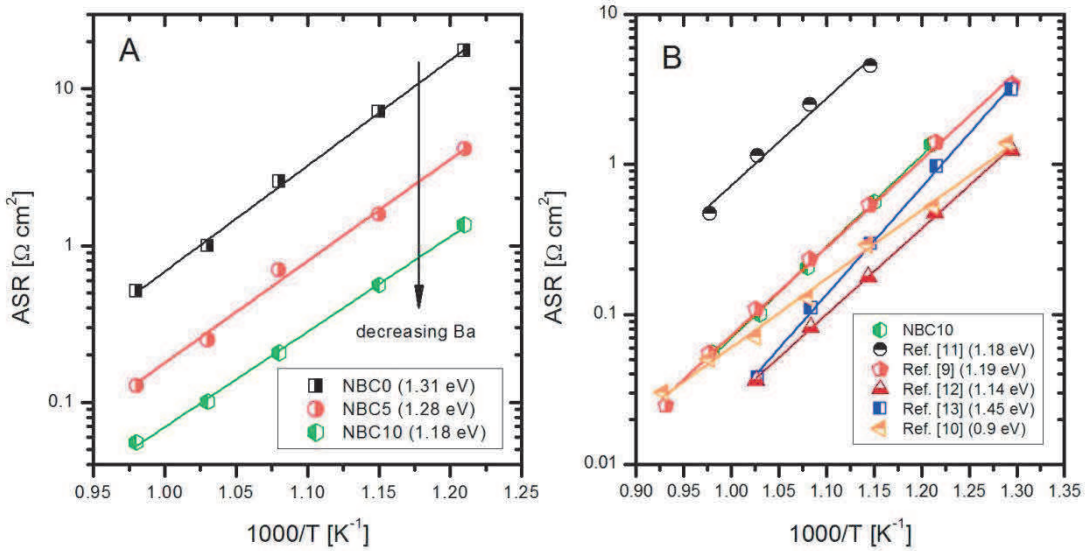
A
B
ASR [Ω cm²]
1000/T [K⁻¹]
decreasing Ba
NBC0 (1.31 eV)
NBC5 (1.28 eV)
NBC10 (1.18 eV)
NBC10
Ref. [11] (1.18 eV)
Ref. [9] (1.19 eV)
Ref. [12] (1.14 eV)
Ref. [13] (1.45 eV)
Ref. [10] (0.9 eV)

Figure 8

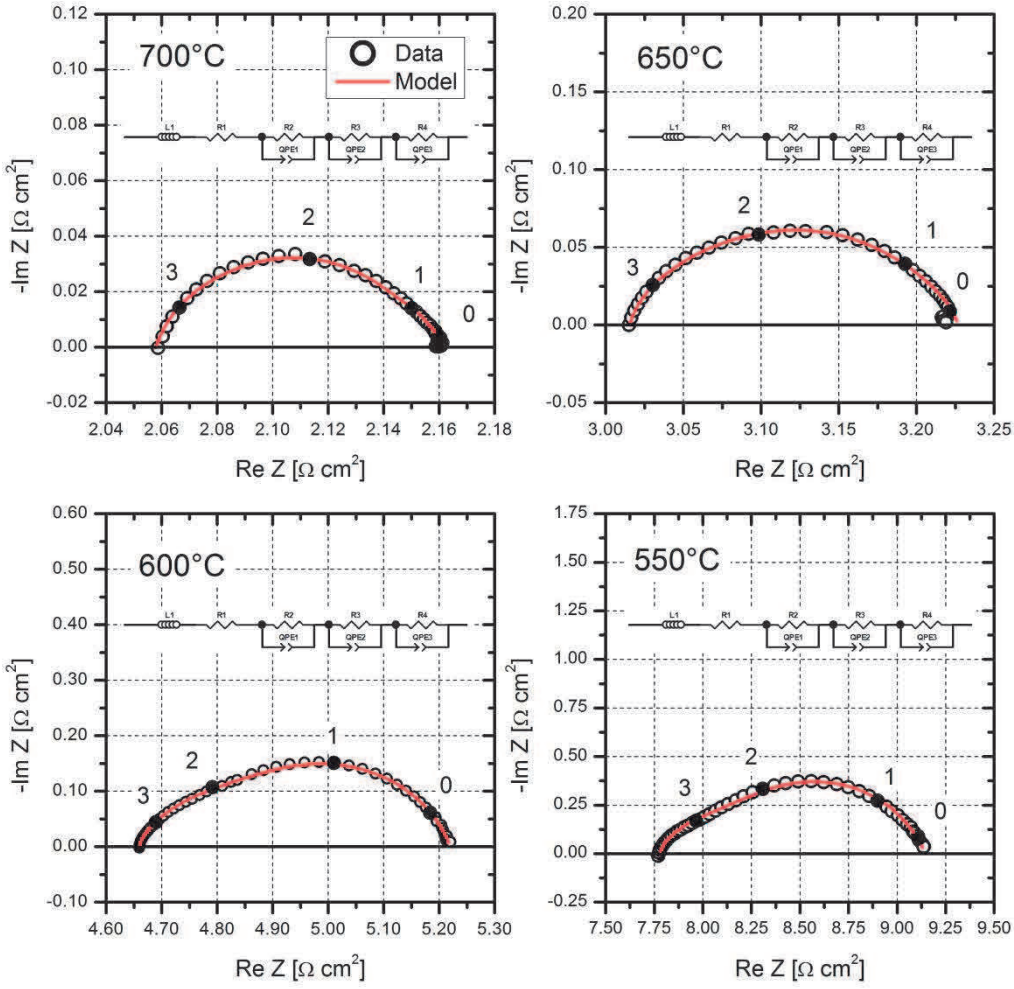
700°C
Data
Model
650°C
600°C
550°C
-Im Z [Ω cm²]
Re Z [Ω cm²]
L1
R1
R2
R3
R4
QPE1
QPE2
QPE3
0
1
2
3

Figure 9

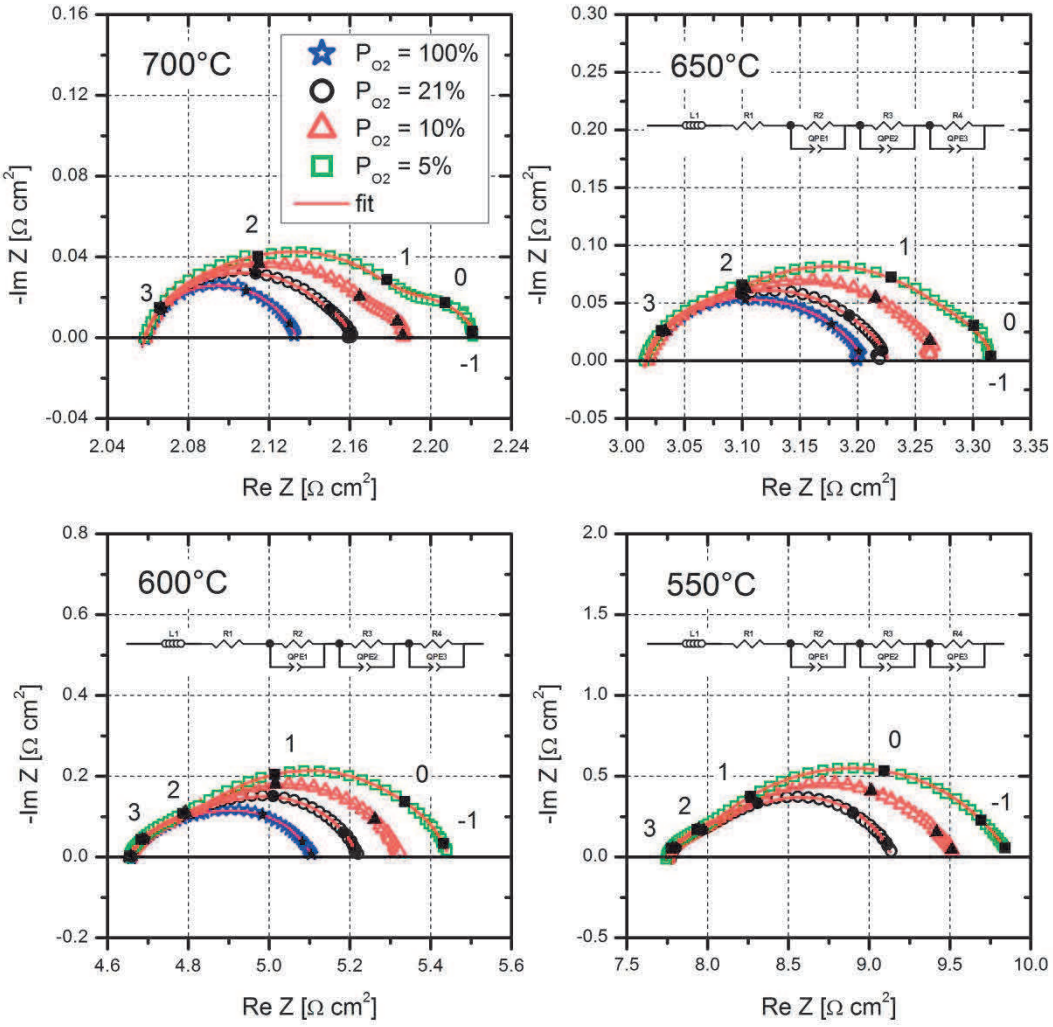
700°C
650°C
600°C
550°C
P$_{O2}$ = 100%
P$_{O2}$ = 21%
P$_{O2}$ = 10%
P$_{O2}$ = 5%
fit
-Im Z [Ω cm^2]
Re Z [Ω cm^2]
L1
R1
R2
R3
R4
QPE1
QPE2
QPE3
0
1
2
3
-1

Figure 10

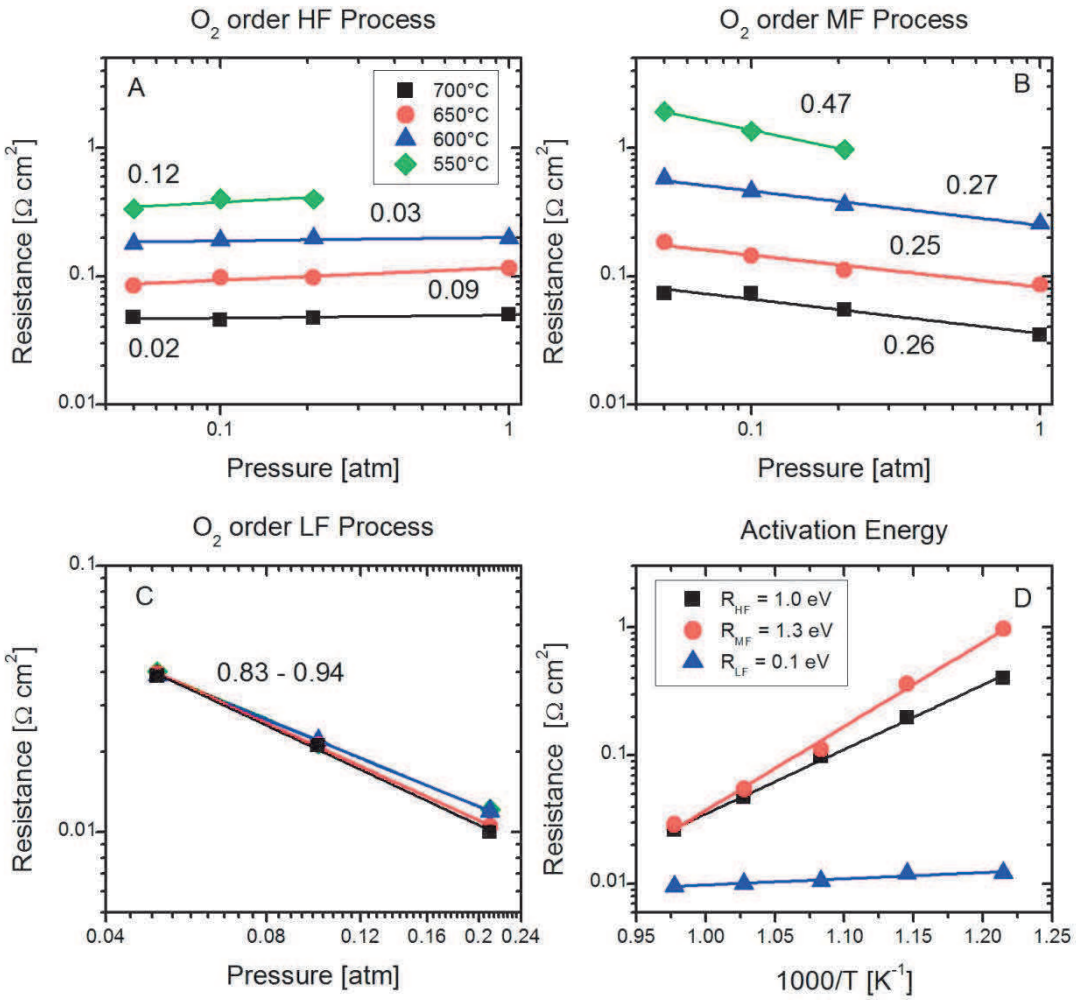
O2 order HF Process
A
700°C
650°C
600°C
550°C
0.12
0.03
0.09
0.02
Resistance [Ω cm2]
Pressure [atm]
O2 order MF Process
B
0.47
0.27
0.25
0.26
Resistance [Ω cm2]
Pressure [atm]
O2 order LF Process
C
0.83 - 0.94
Resistance [Ω cm2]
Pressure [atm]
Activation Energy
D
RHF = 1.0 eV
RMF = 1.3 eV
RLF = 0.1 eV
Resistance [Ω cm2]
1000/T [K-1]

Figure 11

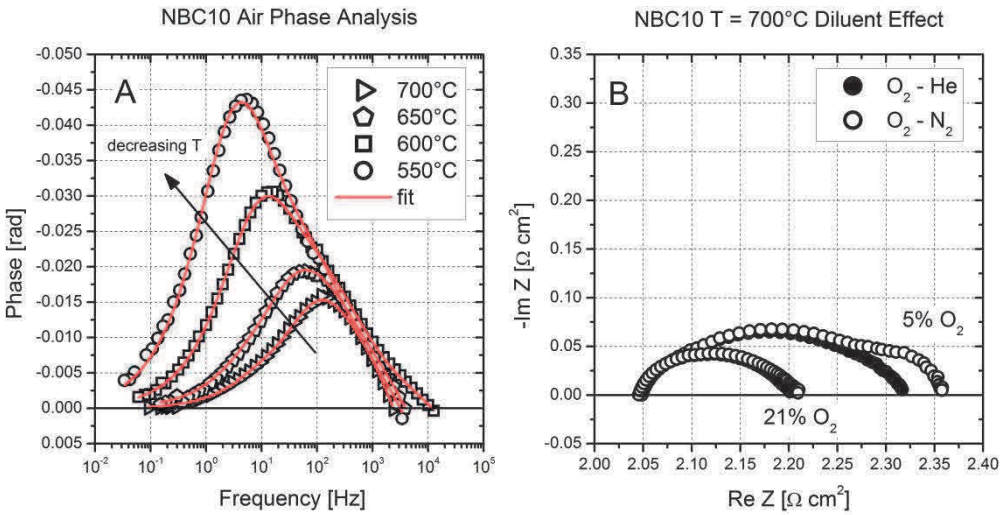
NBC10 Air Phase Analysis
A
decreasing T
700°C
650°C
600°C
550°C
fit
Phase [rad]
Frequency [Hz]
NBC10 T = 700°C Diluent Effect
B
O2 - He
O2 - N2
5% O2
21% O2
-Im Z [Ω cm2]
Re Z [Ω cm2]

Figure 12

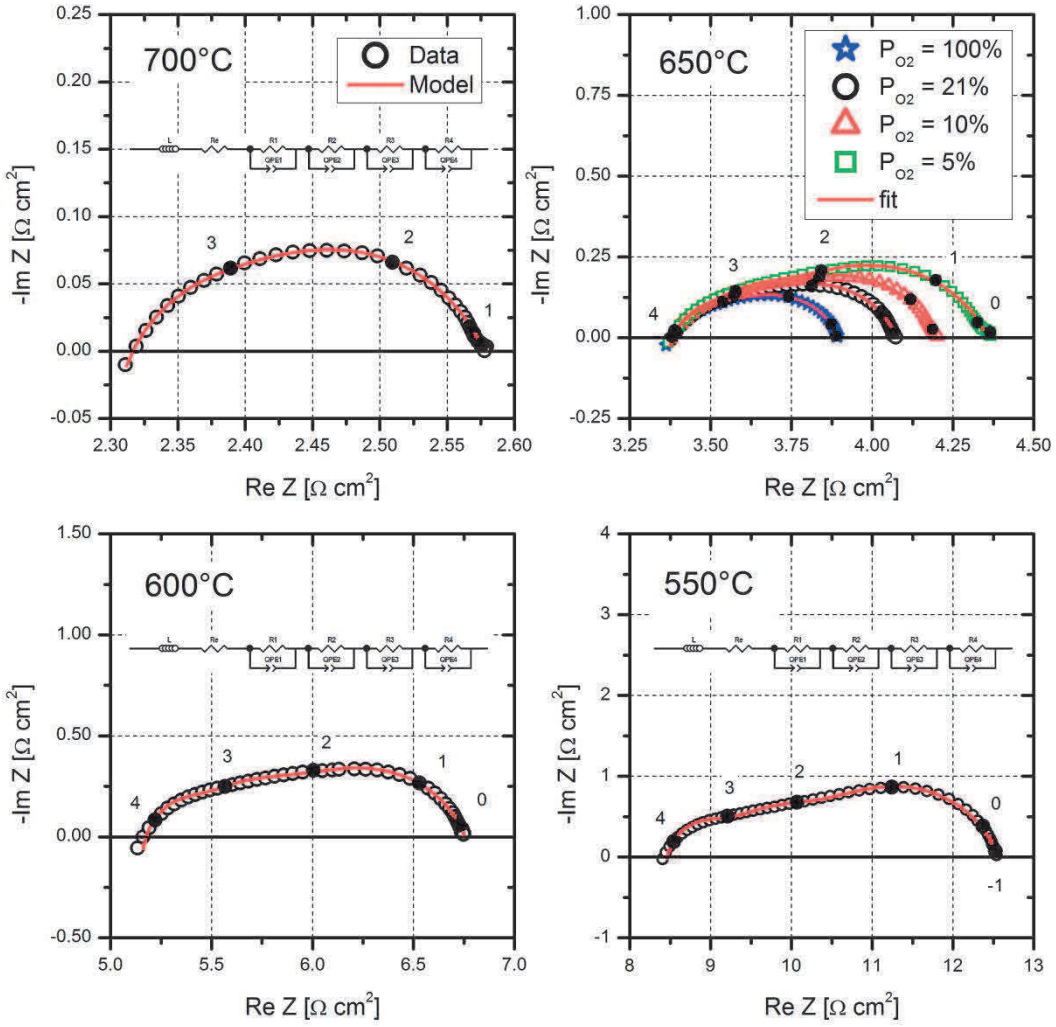
700°C
Data
Model
650°C
P_{O2} = 100%
P_{O2} = 21%
P_{O2} = 10%
P_{O2} = 5%
fit
600°C
550°C
-Im Z [Ω cm^2]
Re Z [Ω cm^2]

Figure 13

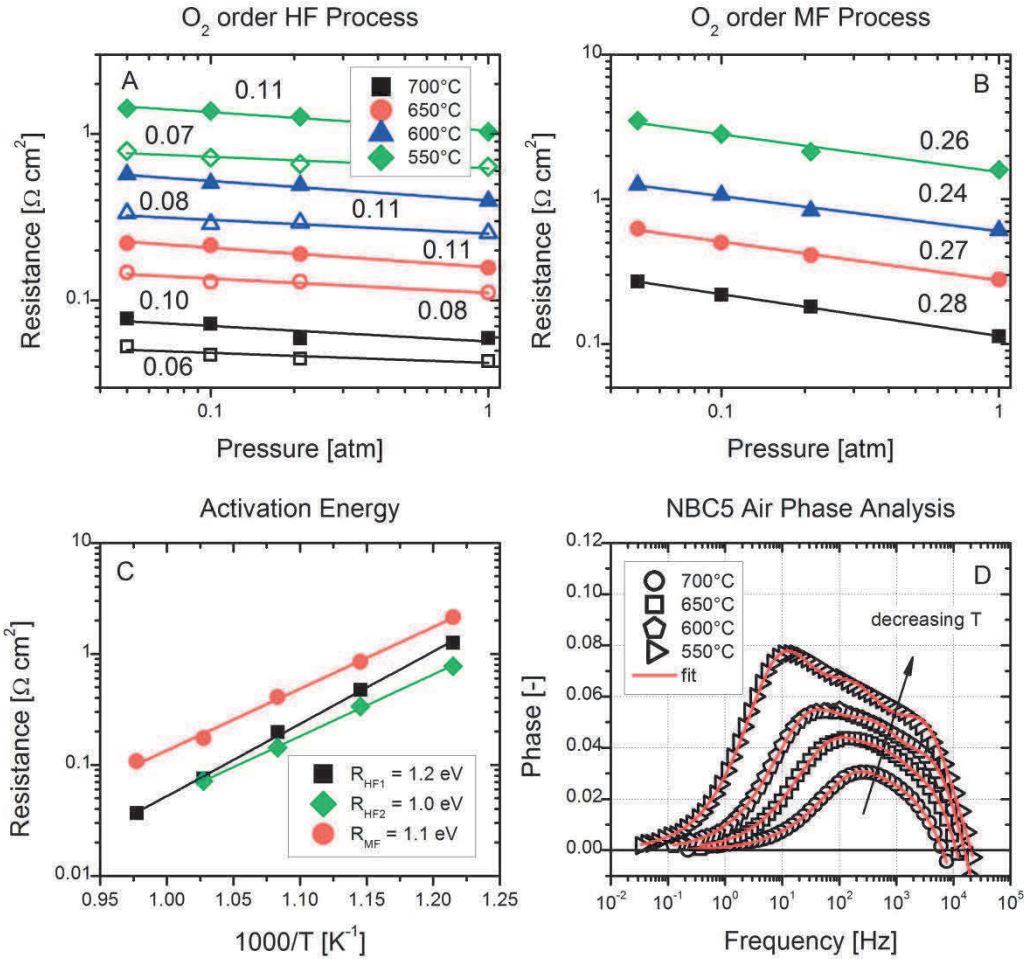
O2 order HF Process
A
0.11
0.07
0.08
0.11
0.11
0.10
0.08
0.06
700°C
650°C
600°C
550°C
Resistance [Ω cm2]
Pressure [atm]
O2 order MF Process
B
0.26
0.24
0.27
0.28
Resistance [Ω cm2]
Pressure [atm]
Activation Energy
C
RHF1 = 1.2 eV
RHF2 = 1.0 eV
RMF = 1.1 eV
Resistance [Ω cm2]
1000/T [K-1]
NBC5 Air Phase Analysis
D
700°C
650°C
600°C
550°C
fit
decreasing T
Phase [-]
Frequency [Hz]

Figure 14

Figure Captions

Figure 1. XRD patterns for the three $NdBa_{1-x}Co_2O_{5+\delta}$ samples. $NdCoO_3$ (PDF #00-025-1064) is marked with *.

Figure 2. Variation of lattice parameters of the $NdBa_{1-x}Co_2O_{5+\delta}$ samples.

Figure 3. SEM micrographs. Panels A and B: NBC10 (a) and NBC20 (b) powders after calcination at 1100°C. Inserts are EDS spectra. Panel C: cross section of the NBC10/GDC/NBC10 cell. Panels D, E and F: cathode/electrolyte interface for the NBC0 (D), NBC5 (E) and NBC10 (F) samples in the symmetric cells.

Figure 4. XRD patterns of NBC/LSGM 50/50 wt% mixture. $LaBaGa_3O_7$ (*). NBC10 (a); NBC5 (b); NBC0 (c).

Figure 5. XRD patterns of NBC/GDC 50/50 wt% mixture. NBC10 (a); NBC5 (b); NBC0 (c).

Figure 6. Panel A: TG curves of the NBC samples. Operating conditions: air flow, T_{ramp} = 3°C/min, T_{MAX}= 850°C. Panel B: variation in the oxygen content with temperature under air flow.

Figure 7. Total electrical conductivity measurements on NBC samples as a function of temperature and Ba deficiency.

Figure 8. Panel A: Arrhenius plot for the ASR of the NBC cathodes in NBC/GDC/NBC cells. Panel B: comparison among ASR values of NBC cathodes taken from the literature.

Figure 9. Complex plane impedance spectra of the NBC10/GDC/NBC10 symmetrical cell measured between 700 and 550°C in flowing air (100 Ncc/min). Operating conditions: open circuit, 10 kHz – 0.1 Hz frequency range. Symbols are data, line is fitting. The logarithm of the frequency decade is indicated.

Figure 10. Complex plane impedance spectra of the NBC10/GDC/NBC10 symmetrical cell measured between 700 and 550°C at varying the O_2 partial pressure between 100% and 5% v/v. Operating conditions: open circuit, 10 kHz – 0.1 Hz frequency range. Symbols are data, line is fitting. The logarithm of the frequency decade is indicated.

Figure 11: NBC10 symmetric cell, T = 550°C – 700°C. Panel A: dependence of the HF resistance on P O_2. Panel B: dependence of the MF resistance on P O_2. Panel C: dependence of the MF resistance on P O_2. Panel D: Arrhenius plot of the resistance of the high frequency (R_{HF}), middle frequency (R_{MF}) and low frequency (R_{LF}) processes under air flow. The absolute value of the slopes is reported.

Figure 12. Panel A: Plot of the phase as a function of the frequency for the NBC10/GDC/NBC10 cell, under air flow condition, at varying temperature between 700 and 550°C. Panel B: effect of the diluent, filled symbols are He, open symbols are N_2.

Figure 13. Complex plane impedance spectra of the NBC5/GDC/NBC5 symmetrical cell measured between 700 and 550°C at varying O_2 partial pressure between 100% and 5% v/v. Operating conditions: open circuit, 10 kHz – 0.1 Hz frequency range. Symbols are data, line is fitting. The logarithm of the frequency decade is indicated.

Figure 14: NBC5 symmetric cell, T = 550°C – 700°C. Panel A: dependence of the HF_1 and HF_2 resistances on P O_2. Full symbols are HF_1 arc, empty symbols are HF_2. Panel B: dependence of the MF resistance on P O_2. Panel C: Arrhenius plot of the resistance of the high frequency (R_{HF1} and R_{HF2}), middle frequency (R_{MF}) and low frequency (R_{LF}) processes under air flow. Panel D: plot of the phase as a function of the frequency, under air flow condition, at varying temperature between 700 and 550°C. The absolute value of the slopes is reported.

Graphical Abstract (for review)

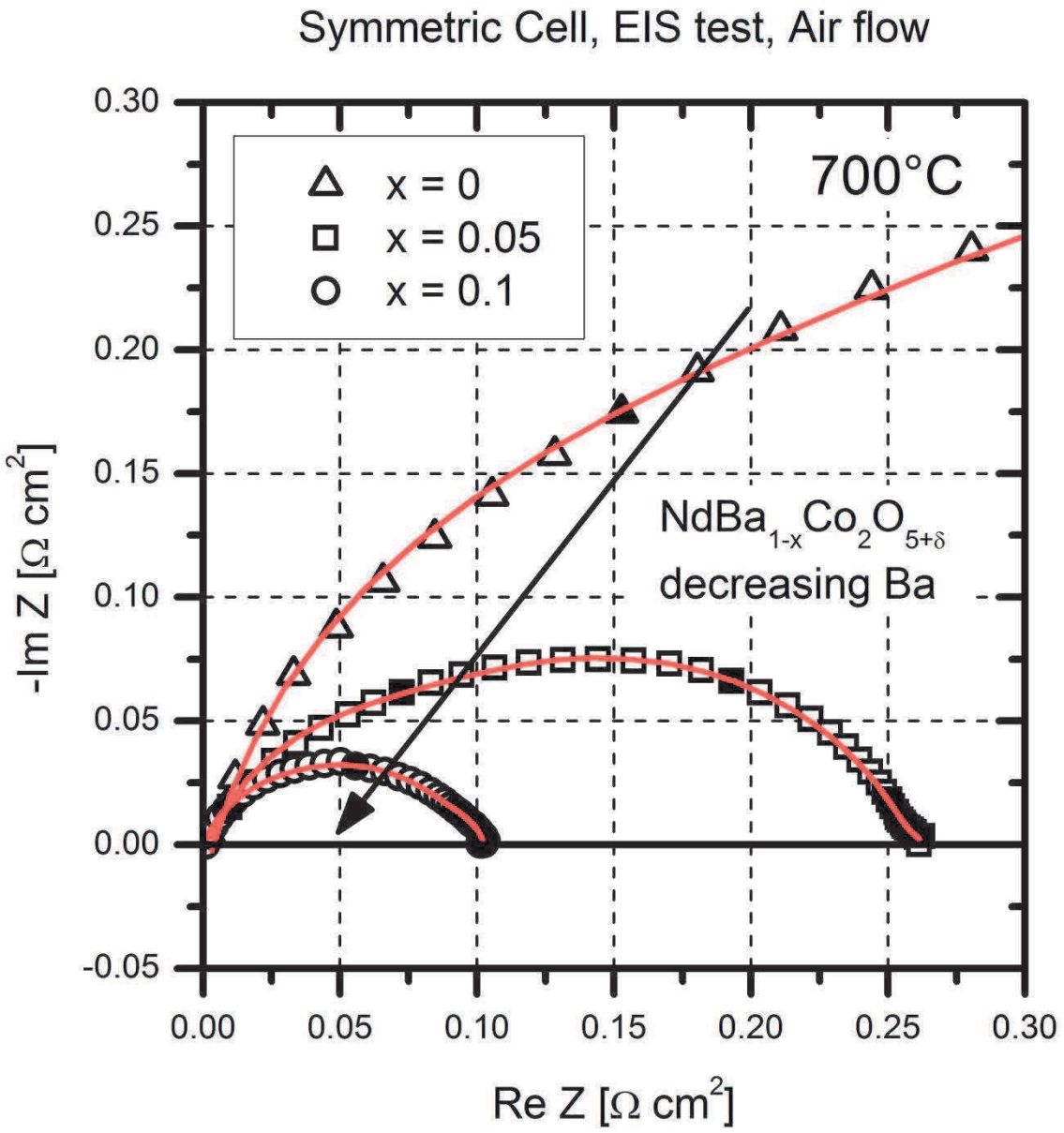

Research Highlights

- Nd-based IT-SOFC cathodes are chemically and electrochemically characterized
- Increasing the Ba deficiency promotes the activity and reduces the polarization
- Detailed EIS investigation on symmetric cells elucidates the kinetic role of Ba
- A polarization resistance of 0.1 Ωcm^2 at 700°C is achieved with 10% Ba deficiency